INTEGRIN ADHESION RESPONSE TO CHEMICAL AND MECHANICAL STIMULATION

A dissertation

by

Huang Huang

Advisor: Gerald A. Meininger Ph.D

Department of Medical Pharmacology and Physiology

December 2017

The undersigned, appointed by the dean of the Graduate School, have examined the dissertation entitled

INTEGRIN ADHESION RESPONSE TO CHEMICAL AND MECHANICAL STIMULATION

Presented by Huang Huang,

a candidate for the degree of doctor of philosophy of physiology,

and hereby certify that, in their opinion, it is worthy of acceptance.

Gerald A. Meininger

Heide Schatten

Michael Hill

Ronald J. Korthuis

ACKNOWLEGEMENTS

I want to express my great respect and deep admiration to my advisor Dr. Gerald A. Meininger. He provided me the opportunity to explore this exciting research field with full support. For the past 6 years, he taught me how to think, write and work as a scientist. I am always amazed by his deep insight of research and inspired discussions with him. He is also a good friend to me with whom I can share my joys and depressions. I will miss our lunch meeting very much. I will be forever grateful for his guidance and friendship during my graduate career.

I would like to thank all the members of my research committee for their help and guidance: Dr. Heide Schatten, Dr. Michael Hill, and Dr. Ronald Korthuis. I have learned a lot about science and life from them all and it is privilege to know them.

Special thanks to Dr. Ronald Korthuis as Head of the Department and Dr. Allan Parrish as Director of Graduate studies. I could not complete my graduate education without their support. The support they provide to the students is so valuable that I am convinced there is no graduate education better than that I received.

I would like to extend special thanks to Dr. Zhe Sun in our group. He taught me how to operate AFM and almost all other techniques from isolating vessels to confocal imaging. Also, I would like to express my appreciation to the former and present members who helped me: Dr. Zhongkui Hong, Dr. Yi Zhu, Dr. Leike Xu, and Zhaohui, Li.

I would also like to thank all faculty, staff and students of our department and Dalton for making my graduate education a memorable one.

Thanks to my parents Shuqin Zheng and Zefei Huang. I’m in their debt that never can pay back for their unconditional love, support and help. I hope I make them proud.

TABLE OF CONTENTS

LIST OF FIGURES

CHAPTER I

INTRODUCTION

BACKGROUND OF INTEGRIN

The vertebrate vascular network is a closed system that functions to circulate nutrients, oxygen, and immune cells to all tissues in the body and to transport metabolites. According to the WHO, cardiovascular disease is a major cause of death worldwide [1]. As one of the major constituents of blood vessel walls, vascular smooth muscle cells (VSMCs) are responsible for the maintenance of vessel structure and function. VSMCs are surrounded by basement membranes that consist of a large number of extracellular matrix (ECM) proteins, which facilitate normal nutrition and metabolisms of arterial VSMCs [2]. ECM contains a variable proportion of a large variety of matrix and non-matrix proteins, providing a mechanical framework, facilitating intercellular communication, and promoting wound healing [3-5]. Extracellular matrices are composed of fibrous proteins (collagens and elastin) embedded in a gel-like polysaccharide ground substance (glycosaminoglycans and proteogylcans) and adhesion proteins that link components of the matrix both to one another and to attached cells (fibronectin, laminin and entactin) [6]. ECM composition notably influences its mechanical properties and is variably expressed throughout the vascular hierarchical network [7, 8]. In large arteries, ECM is composed of elastin which is arranged in fenestrated sheets or lamelle into a three-dimensional continuous network between collagen fibers and thin layers of proteoglycan-rich ECM, while arterioles contain endothelial cells and VSMCs with less elastin and collagen [9]. Though currently there is little known about

the nanoscale organization of the ECM and how it is regulated in the vascular wall, EMC composition is known to be regulated through synthesis and degradation, which is reported to change in pathological conditions [10, 11]. For example, hypertension is associated with increased arterial stiffness characterized by fissuring and fracturing of elastin and collagen proliferation [8].

The ECM is physically linked with cells through transmembrane proteins called integrins, which connect the ECM to the cell cytoskeleton. Integrin proteins are heterodimers formed by the non-covalent association of two subunits, designated α and β [6]. In the vascular system, VSMCs have been reported to express 13 of the approximately 24 known integrins: $\alpha_1\beta_1$, $\alpha_2\beta_1$, $\alpha_3\beta_1$, $\alpha_4\beta_1$, $\alpha_5\beta_1$, $\alpha_6\beta_1$, $\alpha_7\beta_1$, $\alpha_8\beta_1$, $\alpha_9\beta_1$, $\alpha_v\beta_1$, $\alpha_v\beta_3$, $\alpha_v\beta_5$, and $\alpha_6\beta_4$ [12]. A large number of studies from our laboratory have shown integrin involvement in controlling vascular functions, which has been well addressed in reviews by Martinez-Lemus [13, 14]. Adhesion of integrin to extracellular matrix is a highly dynamic process, which is well addressed in Figure 1-1 [15]. Integrins are expressed and remain in a low-affinity binding state until cellular stimulation activates and transforms them into a high-affinity form. One important mechanism for regulating integrin function is through tight spatial and temporal control of integrin affinity for extracellular ligands, which is achieved by rapid, reversible changes in the conformation of the extracellular domains of the integrin heterodimers, termed ‘integrin activation’ [16]. This affinity-dependent mechanism combines with additional affinity-independent mechanisms (such as integrin clustering, lateral diffusion of receptors, interactions with and reorganization of the cytoskeleton, and changes in integrin expression patterns) to control integrin-mediated adhesion [16-19]. Changes in integrin activation

are reported in angiogenesis and altered regulation of integrin activation is evident during impaired cardiac function, suggesting the importance of integrin-mediated cell adhesion in a variety of normal and pathological conditions [20, 21]. In VSMCs changes in integrin expression and adhesion have both been associated with vascular diseases [22-24]. VSMCs, like all tissues in the body, are subjected to dynamic stimuli from the surrounding microenvironment or cells themselves, indicating integrin-mediated VSMCs attachment to ECM is also undergoing dynamic regulation. However, the importance of dynamic behavior is not completely understood in VSMCs and additional research is needed for better understanding vasculature and providing possible pathological targets.

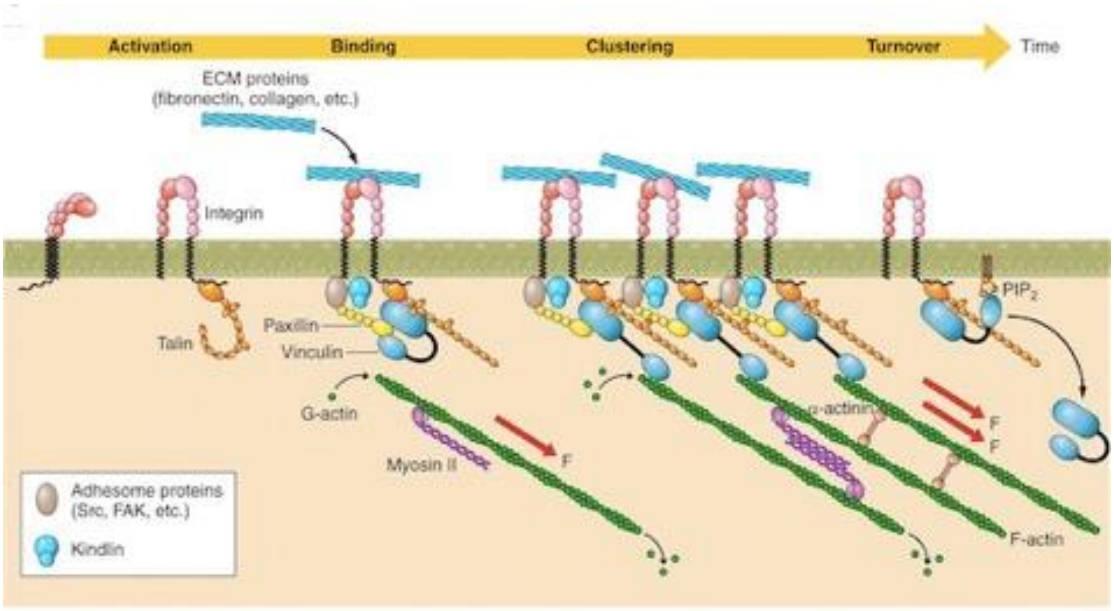

Figure 1-1. Dynamics of focal adhesion formation. In resting state, integrins are present on VSMCs in an inactive 'bent' conformation. Upon outside-in cell signaling there is recruitment of talin to the membrane that binds to the integrin tail and makes integrin to adopt an extended conformation that has high affinity for specific ECM protein ligands. After binding to ECM ligands, the integrin connects to actin filaments through activation of vinculin to promote formation of a nascent focal complex that matures into a focal adhesion. Maturation involves clustering of integrins and recruitment of additional cytoskeletal focal adhesion proteins. Focal adhesion turnover also occurs and is regulated by disassembly of the actin cytoskeleton and loss of interaction of vinculin with

PIP2. Source: Lacolley, P., et al., *Vascular Smooth Muscle Cells and Arterial Stiffening: Relevance in Development, Aging, and Disease.* Physiol Rev, 2017. **97**(4): p. 1555-1617.[15]

VASCULAR STIFFNESS

Arterial stiffness, as one of the earliest detectable manifestations of adverse structure and functional changes within the vessel wall, increases with advancing age and is an independent predictor of cardiovascular morbidity and mortality [25, 26]. The elastic properties of the arterial wall material depend not only on the vascular cells, including ECs and VSMCs, but also ECM and how these components are spatially organized [27]. The methodology for measuring arterial stiffness depends on the size of the artery and its location along the arterial tree. Due to the incompressibility of the blood and the distensibility of the arteries, the pulse generated by the heart travels at finite wave speed along the arterial network. By measuring the pulse wave velocity (PWV), it can be used as good indicator for measurement of vascular stiffness. According to the Moens-Korteweg equation, the PWV is related to the square root of the elasticity modulus. The elastic modulus increases in stiffer arteries as does the PWV. Clinically, carotid-femoral pulse wave velocity is used as the gold standard for the measurement of aortic stiffness [28]. Based on this technique, it has been shown PWV practically doubles form a value of ~5 m/s at the age of 20 to over 10 m/s at the age of 80, which implies that distensibility of the aorta is reduced by 4 over that age range [29]. Recently, improved techniques based on PWV broaden utility of this methods, such as combined with magnetic resonance imaging. However, techniques for measuring stiffness in smaller vessels are much less developed and study of the biomechanical properties of small arteries relies on ex vivo techniques such as isolated vessels, vessel rings

and vessel strips [15]. Although changes in vascular stiffness are largely believed to be due to changes in the composition and organization of the ECM [9], VSMCs have also been shown to stiffen with age and hypertension [30, 31]. Thus, the VSMC itself can contribute to overall changes in the vascular wall with stiffening. In addition, VSMC contractile tone also stiffens the artery wall. The changes in VSMC stiffness are intriguing and it remains an important question to determine whether the cellular changes occur in response to the stiffening of the ECM or whether the cellular changes in stiffness precede the ECM changes. To address this complex question more studies are needed of the longitudinal development or time course of vascular stiffening. In addition, mathematical models of the integrin interactions that occur with the ECM could provide valuable insight useful in designing appropriate biological experiments. One of the important goals of the research in this dissertation was to use a mathematical model to predict integrin adhesion behavior in response to pulsatile changes in stretch applied to integrin-ECM adhesions.

CYTOSKELETON IN VSMCS

The cytoskeleton in VSMCs, like all eukaryotic cells, is composed of three principal types of protein filaments: actin filaments, intermediate filaments, and microtubules, which are held together and linked to subcellular organelles and the plasma membrane by variety of accessory proteins [32]. In addition to serving as a scaffold for providing cellular structural framework, the cytoskeleton is also responsible for internal transportation of organelles and proteins. Importantly, the cytoskeleton is a dynamic structure that is continually reorganized as cells grow, move and change shape.

Actin is the major cytoskeletal protein in cells, and it exists in both a soluble monomeric form (G actin) and a polymeric filamentous state (F actin) [32]. The soluble free cytosolic actin monomers are constantly exchanging with actin monomers within the actin filaments. In VSMCs, actin filaments are anchored to the membrane via a complex of adhesion proteins via integrins, cadherins and at cytosolic dense bodies that are composed primarily of the actin cross-linking protein, α-actinin [33]. During actin filament assembly two patterns of filament formation are observed. One is formation of branching structures and the other involves changes in filament length such as elongation. Remodeling of the actin network is a constant feature of this cytoskeletal component and it is facilitated by actin depolymerization and debranching both of which facilitate dynamic remodeling. In contractile VSMCs, stress fibers are also assembled and act as contractile/structural bundles containing actin filaments and myosin II [34]. In addition to well established actomyosin interaction that leads to contraction, dynamic remodeling of the actin cytoskeleton is also recognized as an important step in the agonist-induced activation of contraction and tension development [33, 35]. Actin dynamics can be regulated by multiple actin-associated proteins and many intracellular signaling pathways. RhoA has been reported to promote actin nucleation and stress fiber assembly by activating mammalian Diaphanous-related formins (mDia) [36]. LIM kinase is another target of RhoA/RhoK pathway, which phosphorylates cofilin, leading to actin polymerization [37, 38].

Intermediate filaments (IFs) are also widely distributed in the cytoplasm, and type III IF proteins vimentin and desmin are major components of the IF network in smooth muscle [39]. VSMCs mainly express vimentin, which is

widely distributed in various blood vessels ranging from elastic arteries to arterioles in the microcirculation while desmin is not or very little detected in large arteries such as aorta, but mainly present in arterioles [39, 40]. Traditionally, IFs are considered not directly involved in cell movements, but rather they appear to play a structural role by providing mechanical strength to cells and tissues [32]. However, recent studies suggest IF network is an essential component for force development in smooth muscle and that contractile activation induces partial disassembly of vimentin and/or desmin filaments, and spatial rearrangement of vimentin to modulate force development through the redistribution of signaling molecules [41].

Microtubules are long and hollow cylinders made up of α- and β-tubulin dimers, which bind in a head-to-tail manner into protofilaments that associate laterally to from hollow tubes [32]. They are essential for cell shape and variety of cell movements, including cell division and the intracellular transport of organelles and vesicles. It has been shown that microtubules regulate focal complex assembly/disassembly, protrusion and cell contraction locally [40]. In arterioles, microtubule depolymerization induces an increase in RhoA activity and causes constriction [42]. In VSMCs, it is also reported that microtubule stabilization attenuates cell calcification [43].

CONTRACTILE ACTIVATION PATHWAYS IN VSMCS

VSMCs display considerable plasticity in phenotype such that in healthy blood vessels mostly exhibit the contractile phenotype but switch frequently switch to a synthetic, largely non-contractile phenotype in cardiovascular diseases [44]. The synthetic phenotype being dominated by proliferative and migratory characteristics. Contractility of VSMCs is key to its principle function

related to regulating vascular resistance which determines arterial blood pressure. The ability of VSMC to contract and regulate vascular caliber results from the contractile filaments composed of actin and myosin which undergo complex molecular interactions that allow the VSMC to shorten thereby affecting vascular radius. According to Poiseulle's law blood flow and pressure are sensitive to the radius to the fourth power making adjustments in vascular diameter a powerful way to regulate blood flow and pressure. In VSMC, actin and myosin filaments are gathered into loose bundles unlike the highly structure arrays of actin and myosin found in skeletal and cardiac muscle [34]. These bundles are anchored to dense bodies in the cytosol and to attachment plaques at cell membrane. Myosin II, is a major molecular motor present in muscle cells, consisting of two identical heavy chains (MHC) and two pairs of light chains (MLC). Myosin bind to actin filaments in a reversible fashion allowing the myosin to move along the actin filaments creating a sliding of actin filaments relative to each other. This interaction generates contraction by hydrolyzing ATP. Phosphorylation of 20-kDa MLC has been identified as an essential event for actomyosin interaction [34]. This is controlled by Ca^{2+} and Rho kinase signaling pathways. Intracellular Ca^{2+} can be increased either from extracellular Ca^{2+} influx through opening of voltage-gated Ca^{2+} channels or release from intracellular stores via sarcoplasmic reticulum. Opening of stores occurs via activation of G protein-coupled receptors and subsequent inositol triphosphate (IP_3) productions. MLC has been known to be phosphorylated at Ser19 mediated by Ca^{2+}/calmodulin-activated myosin light chain kinase (MLCK), which in turn promote actomyosin interaction and contraction [34, 44]. VSMCs is highly spatially organized with respect to its organelles and signaling

pathways. This compartmentalization regulates Ca^{2+} signals that regulate contractility as well as other intracellular functions in a more selective manner. MLC could also be regulated by dephosphorylation which is Ca^{2+} independent. This regulation is mediated by a specific type 1 myosin light chain phosphatase, MLCP, which is a heterotrimer consisting of a catalytic subunit and a regulatory subunit, known as myosin phosphatase target subunit (MYPT1). Activation of Rho-family small GTPase with their downstream effectors (Rho-associated protein kinase, RhoK) activates phosphatase MYPT1, that inhibits MLCP activity [45]. Activation of PKC and/or RhoA/RhoK signaling pathway thus results in Ca^{2+} sensitization of contractile proteins and thereby tonic VSMC contraction despite decreased levels of intracellular Ca^{2+} [46].

ANGIOTENSIN II SIGNALING IN VSMCS

Angiotensin II (AII) is an important hormone regulated by the renin-angiotensin system. It is a powerful vasoconstrictor and regulates VSMC function via binding to its cell-surface receptors AT_1R and AT_2R, which belong to the G proteins coupled seven trans-membrane superfamily [47]. In vessels, the AT_2R has been reported less localized on the VSMCs but is mainly expressed in adventitial cell types [48]. AT_1R is the major receptor that mediates most of the physiological and pathophysiological effects of AII, including vasoconstriction, inflammation, growth, and fibrosis [49]. It is suggested that AT_2R may counteract many of the AT_1R-mediated actions. When AII binds to the Gq/G11 coupled AT_1R it results in activation of many intracellular signaling pathways, including PLC, Ca^{2+} channels, MAP kinases, NADH oxidase and others as well as alterations in gene expression leading to changes in protein expression within the cell [50].

AII-induced contraction in VSMCs is mediated by both Ca^{2+} dependent and Ca^{2+} independent pathways [51]. It is well established that AII binding to AT_1R activates PLC isoforms to generate second messenger, IP3 and DAG. IP3 in turn is well known to induce calcium release from sarcoplasmic reticulum via the ryanodine receptor (RyR). Voltage-dependent calcium channels are also reported to be activated directly or indirectly by AII. DAG mediates VSMCs contraction through activation of protein kinase C (PKC), which in turn phosphorylates MLCK leading to activation of several other target proteins promoting contraction [52].

The MAPKs have also been implicated in AII induced VSMC proliferation, hypertrophy and differentiation [53]. The extracellular signal-regulated kinase 1 and 2 (ERK1/2), the c-Jun N-terminal kinase (JNK), p38 MAPK, and big MAPK1 (BMK1 OR ERK5) have all been identified to play an important role in these functions [54, 55]. The ERK1/2 pathway exerts a hypertensive action induced by AII through triggering MLCK and thereby MLC phosphorylation. AII has been known to induce phosphorylation of multiple tyrosine kinases, including c-Src, janus family kinase (JAK), focal adhesion kinase (FAK), Pyk2, p130Cas and phosphatidylinositol 3-kinase (PI3K). Activation of RhoA/Rho-kinases signaling also has been reported in AII-stimulated VSMCs [56-58].

As a potent stimulator of vascular NAD(P)H oxidase, AII mediates many of its effects by stimulating production of reactive oxygen species (ROS) [59, 60]. Of the many types of ROS generated, superoxide anion ($\bullet O_2^-$), hydrogen peroxide (H_2O_2), nitric oxide (NO) and peroxynitrite (ONOO-) are particularly important in the cardiovascular system. It's reported that AII induces activation

of the enzyme NAD(P)H oxidase as well as increase expression of its subunits. It also stimulates ROS production in cultured VSMCs and intact arteries. ROS influences many intracellular signaling such as MAP kinase, tyrosine kinases and protein phosphatase while upstream signaling molecules including PLD, PKC, c-Src, PI3K and Rac [61]. Thus, AII signaling in VSMC is extremely intricate involving many potential pathways either directly or indirectly. It ability to initiate Ca^{2+} signaling was an important focus of the research presented in this dissertation.

RATIONALE

The mechanical properties of VSMC is determined by the cytoskeleton, that is resulted from both dynamic actomyosin interactions as well as by the capacity of the actin cytoskeleton to rapidly depolymerize and reploymerize [30, 31, 62]. Furthermore, VSMC mechanics have been shown to be dependent on cell-matrix adhesion [63-65] and recent evidence from our laboratory showed that integrin adhesion is coordinated with VSMCs stiffness, which can be rapidly up-regulated with contraction and downregulated during relaxation in response to vasoactive agents [66]. However, the mechanisms governing dynamic response to agonists have not been completely understood.

Therefore, the first project of this research focused on possible mechanisms governing this dynamic behavior of adhesion in response to agonists and changes in VSMC stiffness. Studies of the myogenic response in resistance vessels reveal an overlap between calcium signaling and integrin-signaling pathways in VSMC [13, 67]. Ligands of the $\alpha_5\beta_1$ and $\alpha_4\beta_1$ integrin produce significant enhancement of L-type calcium current while ligands of the $\alpha_v\beta_3$ integrin cause a decrease in VSMC($[Ca^{2+}]_i$ [68-70]. Collectively, these

data implicate a role of integrin in intracellular calcium ($[Ca^{2+}]_i$). In project one, we hypothesized that the coordination of cell stiffness and cell adhesion to FN of VSMCs was mediated by changes $[Ca^{2+}]_i$. To address this hypothesis, calcium indicator fluo-4 was used to measure $[Ca^{2+}]_i$ simultaneously with real-time monitoring cell stiffness and adhesion to ECM protein fibronectin (FN). In this study, we found that cell stiffness and cell adhesion to FN are changed directionally with $[Ca^{2+}]_i$.

Project two of this work focused on how integrin adhesion is influenced by dynamic mechanical stimulation. VSMCs from elastic arteries and smaller resistance arteries are exposed to mechanical stretch stress or tension [9, 71]. This cyclic strain stress is created by the pulse pressure. This oscillating stretch is felt by VSMCs through their interaction with ECM mediated by integrins, and can be dissected to contain stretching in both the lateral and vertical directions. In this project, we collaborated with applied mathematical scientists from the University of Nottingham to test a simulation model of integrin adhesion behavior to oscillations. They proposed a 3-spring model to investigate the interaction of integrin and ECM during dynamic stretching of the integrin-ECM adhesion. The model predicted that integrin adhesion outcomes are dependent on initial integrin adhesion and applied oscillation amplitudes. We experimentally verified the dependence of integrin adhesion on these parameters.

AFM APPLIED TO MEASURING CELL MECHANICS AND ADHESION

My research was largely dependent on using atomic force microscopy (AFM). The invention of AFM opened a new area of research that can directly

stimulate cells with local nanoscale forces [72, 73]. By probing biological structures, AFM can obtain images over a large range of length scales such as DNA, proteins, and cellular surface structure with nanometer resolution [74-76]. For imaging, a soft cantilever with a very small tip at the end scanned across the surface of a sample. A laser beam is aligned to the end of the cantilever, which is precisely moved in the xy-direction with a piezoelectric scanner. The cantilever bends in response to surface topography during scanning, thus reconstructing movement of the reflected laser beam would get topographic images of biological structures.

Apart from imaging, AFM force spectroscopy can be used to quantify the mechanical properties and interactions of biological systems over scales form cells to single-molecules [77-79]. In force spectroscopy, AFM cantilever can be moved perpendicular to the cell surface and treated as a spring to get force acted on cantilever by Hooke's law with its spring constant at resolution of pN. In this work, cell mechanics and adhesion were measured by 'force-distance curves' that are recorded by the deflection of the cantilever movement as it approaches to and retracts from a cell surface. During the approach, the cantilever will begin bending upward as it is pushed on the sample, after determining the contact point, the recorded force-distance curve can be converted into force-indentation curve. The cell modulus can be obtained by fitting the force-indentation curve with Hertz model [77].

AFM can also be applied to probe molecular interactions, which enables the measurement of the strength of the interaction forces between the probe and cells [80, 81]. Labelling the tip with chemical groups or bio-ligands will allow AFM a unique opportunity to probe the properties of specific ligand-receptor

complexes [82]. For retraction force curves, AFM tip is retracted while also measuring the force acting on the cantilever. If a molecular interaction exists, the cantilever will bend downwards until the interacting pair of molecules rupture, which produces rupture events. The height of the rupture event corresponds to the force required to break a single molecule interaction, thus to the binding strength of a given receptor. Therefore, AFM-based single cell force spectroscopy is capable of revealing the mechanical and energetic characteristic of single receptor-ligand interactions on the surfaces of living cells. Moreover, spatially resolved force-distance curves can provide a means to localize individual molecules on the cell surface. Additionally, these approaches have also been adapted to measure the mechanical interaction between a single cell and other cells [83].

CHAPTER II

MECHANISMS COORDINATING VASCULAR SMOOTH MUSCLE ADHESION TO THE EXTRACELLULAR MATRIX DURING CONTRACTION

ABSTRACT

Physical coupling of vascular smooth muscle cells (VSMCs) to extracellular matrix proteins (ECM) by integrins is required for efficient mechanotransduction. Integrin adhesion receptors are essential for normal vascular function and defective integrin signaling is associated with cardiovascular disease. There is a large body of accumulated literature on integrin activation in cancer cells and leukocytes, but far less is known about mechanism of integrin activation in VSMCs as it relates to vasoregulation. Previous work from our laboratory demonstrated that increased VSMC stiffness, induced by the vasoconstrictor Angiotensin II (AII), is coordinated with enhanced adhesion to fibronectin (FN) indicating an important role for adhesion in contraction. However, the mechanism of this coordination is not fully understood. In this study, we hypothesized that enhanced adhesion in response to AII was mediated by integrin activation through an inside-out signaling pathway linked to increases in intracellular Ca^{2+} ($[Ca^{2+}]_i$). By using atomic force microscopy (AFM) with an anti-α_5 antibody coated AFM probe, we confirmed that cell stiffness was increased by AII, but we observed no changes in adhesion to the anti-α_5 antibody. This indicated that increases in cell adhesion to FN induced by AII was occurring through an integrin activation process, as increased membrane integrin expression/receptor density would

have been accompanied by increased adhesion to the anti-α_5 antibody. Further studies with KCl and BAPTA-AM were used to modulate the level of $[Ca^{2+}]_i$. After KCl, VSMCs showed a rapid transient increase in cell stiffness as well as cell adhesion to FN, and these two events were synchronized with superimposed transient increases in the level of $[Ca^{2+}]_i$, which was measured using the Ca^{2+} indicator, fluo-4. These changes were not abolished in VSMCs pretreated with the myosin light chain kinase inhibitor, ML-7. In contrast, VSMCs incubated with intracellular calcium chelator, BAPTA-AM, showed reductions in stiffness and cell adhesion to FN as well as decreased $[Ca^{2+}]_i$. These data suggest that in VSMCs integrin activation is regulated by levels of $[Ca^{2+}]_i$ and is not dependent on events downstream of contraction. These findings provide additional evidence to support a role for adhesion in VSMC contraction and suggest that following cell contractile activation, that adhesion may be regulated in tandem or even in advance of the contractile event.

INTRODUCTION

Normal cardiovascular function depends on the biomechanical properties of blood vessels, and changes in these properties are characteristic of diseases including hypertension, stroke, aneurysms, atherosclerosis and heart disease [84]. The mechanical properties of a blood vessel are determined by its components and their organization. Accordingly, the stiffness of vascular tissue can be derived from the composition of the extracellular matrix (ECM) and the cells in the tissue, the organization of the matrix and cells, and the connections that link these components (cell-matrix and cell-cell contacts) [85]. It is commonly accepted that changes in the ECM predominately mediate vascular stiffness, that decreased elastin and increased collagen have been

identified as the most altered ECM components [7, 10]. In addition to the ECM, it has been recently established that vascular smooth muscle cells (VSMCs), as the main cellular constituent of the vascular wall, are also recognized to be associated with reduced flexibility and increased stiffness of the blood vessel wall. For example, Sehgel et al. [30] found increased elastic stiffness of VSMCs in spontaneously hypertensive rats, and Zhu et al. [31] have demonstrated higher stiffness in VSMCs from old monkeys than young monkeys. Cytoskeletal proteins, and contractile states have been proved to mediate cell stiffness in VSMCs [62, 66, 86]. In these studies, VSMC adhesion to ECM proteins was also shown to be enhanced as well as cell stiffness. Fibronectin (FN) is one of the major ECM proteins that promotes adhesion of VSMCs to ECM by binding to integrin receptors through functional specialized domains such as arginine-glycine-aspartate (RGD sequence), reported to accumulate in diseased artery walls [87]. Of importance, the $\alpha_5\beta_1$ integrin is recognized as a major FN receptor and plays an important role in VSMCs mechanoreception linking it to vascular regulation [88, 89].

Integrins, as heterodimeric membrane receptors composed of two noncovalent associated transmembrane subunits –α and -β, provide an important physical connection between the ECM and the cytoskeleton, maintaining a dynamic adhesion between the cell and its microenvironment. This unique feature of integrins make them ideally situated for bi-directionally transmitting mechanical forces and the generation of cell signals through both inside-out and outside-in mechanisms. Integrins are known to regulate cell differentiation, proliferation, and survival through controlling critical intracellular signals [90-92]. Accumulated evidence has demonstrated that an important role

for integrins in regulating vascular function [93-95]. Among the multitude of integrin receptors identified on the surface of VSMCs, integrin $\alpha_5\beta_1$ acts as the dominant FN receptor [87, 88, 96]. In previous work from our laboratory, Hong et al. demonstrated the existence of coordination between cell stiffness and cell adhesion of VSMCs to FN as they respond to the contractile vasoactive agonist Angiotensin II (AII) or to the vasodilators adenosine and nitric oxide [66, 97]. This coordination of adhesion with the contractile state was suggested to be regulated by changes in integrin behavior [66]. The function of integrin can be controlled by both 'outside-in' signaling and 'inside-out signaling' [98]. In the case of VSMC activation by soluble vasoactive agonists it is likely that changes in the integrin activation state are occurring through an 'inside-out activation' process from within the cell. Such changes in integrin activation occur through conformational changes in the extracellular integrin head domains in which they can switch reversibly from a low-affinity conformation to a high-affinity active conformation [16]. Integrin $\alpha_5\beta_1$ has been observed to undergo conformational changes in focal adhesions [99], and these changes have been demonstrated to occur with alterations in cytoskeletal tension [100, 101]. However, the mechanism underlying the changes in integrin activation in VSMCs in response to vasoactive-agonists is not fully understood.

In this study, we hypothesized that the coordination of cell stiffness and cell adhesion to FN of VSMCs is mediated by changes in intracellular calcium ($[Ca^{2+}]_i$). Therefore, the enhanced adhesion in response to AII may result from integrin activation through an 'inside-out' signaling pathway linked to an increase in $[Ca^{2+}]_i$. To address this hypothesis, we utilized atomic force microscopy (AFM) combined with confocal microscopy. AFM has the ability to

detect and apply mechanical forces at the nano- and pico-newton ranges, providing a powerful tool for investigating biomechanical properties of VSMCs [102] and for measuring changes in cell adhesion molecules [73, 101, 103]. In this study, AFM was used for real-time monitoring of cell stiffness and adhesion. This allowed us to analyze these variables in the time domain and correlate them with $[Ca^{2+}]_i$, measured using the calcium indicator fluo-4. We show that cell stiffness and cell adhesion to FN are changed directionally with $[Ca^{2+}]_i$. We also observed that increased cell stiffness and adhesion to FN was not abolished by preventing contractile filament interaction via inhibiting myosin light chain kinase (MLCK). Thus, the changes in cell stiffness and adhesion appear to occur by a signaling pathway parallel to but not downstream of contraction.

METHODS

Reagents and Materials applied

For all studies described, human plasma fibronectin (FN), 1, 2-bis(o-aminophenoxy) ethane-N, N, N', N'-tetraacetic acid (acetoxymethyl ester) (BAPTA-AM), and fluo 4-AM were purchased from Invitrogen (Carlsbad, CA, USA), Bovine Serum Albumin (BSA), KCl, AII were purchase from Sigma (St. Louis, MO, USA). Antibodies to α-actin, integrin α5, Angiotensin II type I receptor (AT1R) and phalloidin 647were purchased form Abcam (Cambridge, UK). For all cell isolations, dithioerythriotol (Dith), papain, collagenase, soybean trypsin inhibitor, and elastase were purchased from Sigma (St. Louis, MO, USA). For studies using atomic force microscopy (AFM), a Bioscope II AFM system (Bruker, Santa Barbara, CA, USA) was mounted on an Fluoview confocal microscope (Olympus, Thornwood, NY). AFM data were collected and

analyzed using Nanoscope (Bruker, Santa Barbara, CA, USA) and Matlab (MathWorks, Natick, MA, USA) software. Confocal images were analyzed by using ImagePro Plus software (Media Cybernetics, Carlsbad, CA).

Cell preparation

Animal and Tissue preparation

Male Sprague-Dawley rats (200 g-300 g) were used in this study and were maintained in accordance with the protocol of the Guide for the Care and Use of Laboratory Animals (NIH 83-23, revised 1996). The animal protocol was reviewed and approved by the Laboratory Animal Use Committee (ACUC) of the University of Missouri. Animals were housed individually in a 12:12 light-dark cycle with free access to food and water. Arteriole were isolated as descripted in previous work with minor modification [66]. Briefly, rats were anesthetized by intraperitoneal injection of pentobarbital sodium (Lundbeck, Inc., Deerfield, IL, USA) at 0.1 g/kg. A surgical plane of anesthesia was confirmed by observing no spinal reflex to a toe pinch. The cremaster muscle was removed through a scrotal surgical incision while rats remained under anesthesia, and the tissue was immediately placed in cold (4 ^{o}C), Ringer's buffer (composed of 145 NaCl mM, 4.7 KCl mM, 2.0 $CaCl_2$-$2H_20$ mM, 1.0 $MgSO_4$-$7H_20$ mM, 1.2 NaH_2PO_4-H_2O mM, 0.02 EDTA-$2H_2O$ mM, 3.0 MOPS, 5 Glucose mM, 2.0 Pyruvic Acid mM). Vessels and cell isolations were performed in solution based on Ringer's buffer. Anesthetized rats were euthanized by intracardial injection of saturated KCl solution (3 ml). The cremaster muscles were then pinned flat onto a silicone rubber pad in a bath of cold Ringer's buffer. With the aid of a stereomicroscope (Olympus SZX10, Thorwood, NY, USA), long segments of the first and second order cremasteric feed arterioles vessel

were dissected and isolated from surrounding skeletal muscle tissue. The isolated arteriole segments were removed and cut into small pieces (~2-3 mm) and were placed into culture dishes (35 mm) with Ringer's buffer in room temperature, and subsequently processed to isolate vascular smooth muscle cells (VSMCs).

VSMCs isolation and culture

VSMCs were enzymatically isolated using previously described methods [104]. Briefly, arteriolar segments were transferred to a glass culture tube (10 mm $\times$ 75 mm) that contained 1 ml of the first cell dissociation solution that Ringer's buffer included 27 U/ml of papain and 1 mg/ml dithioerythriotol. The segments were incubated at 37 ^{o}C for 30 minutes without agitation. At the end of this interval, the first cell dissociation solution was carefully decanted and replaced with 1 ml of second cell dissociation solution consisting of Ringer's buffer and 0.5 U/ml collagenase, 75 U/ml elastase, and 1 mg/ml soybean trypsin inhibitor. The segments were further incubated for 12-15 minutes at 37^{o}C. At the end of the incubation period, the dissociation solution was carefully decanted with that not disturb the arteriole segment. Arteriole segments were then very carefully and gently washed twice by adding 1ml Ringer's buffer, followed by 1 ml serum-free supplemented Dulbecco's modified Eagle's medium (DMEM)/F12 (Invitrogen, Carlsbad, CA, USA). The vessels segments were pipetted with a glass pipet (1 ml) for about 20-30 times to disperse individual cells from the tissue. The solution containing the dispersed VSMCs was then decanted into 60 mm tissue culture dishes (Corning incorporated, Corning, NY, USA), and maintained under culture conditions in a humidified incubator with 5% CO_2, at 37 ^{o}C, in DMEM supplemented with 20% fetal bovine

serum (FBS, ATLANTA Biologicals, Laurenceville, GA, USA), 10 mM HEPES (Sigma, St. Louis, MO, USA), 1 mM sodium pyruvate, 2 mM L-glutamine, 100 U/ml penicillin, and 100 g/ml streptomycin. After 48 hours' incubation, the culture medium was changed to DMEM with 10% FBS. The cells used in all experiments were maintained under these conditions for 5-10 days without passage. Prior to an experiment the VSMCs were serum starved overnight.

Force spectroscopy measurement

Bio-functionalized AFM probes

A 5 μm diameter glass bead (Structure Probe Inc., West Chester, PA, USA) was glued on the tip of an AFM probe (MLCT-O10, Bruker Corp., Santa Barbara, CA, USA) and then coated with FN or anti-α5 antibody using the protocol previously used in our Laboratory [88]. Briefly, the bead was first glued on a clean AFM probe and then FN was attached to bead by a cross-linker. Before gluing the glass bead to the cantilever tip, each cantilever was calibrated before a given experiment using thermal noise amplitude analysis. Cantilevers were then cleaned first by rinsing in 100% ethanol twice followed by rinsing in acetone for 3 times. The cantilever was dipped in glue (Progressive Epoxy Polymers Inc., USA) and then brought into contact with a glass bead mixture in solution that had been smeared on a glass slide. After bead attachment, AFM probes were stored for 48 hours to allow bead glue to cure. The AFM probe with attached bead was then processed to bio-coat the bead tip. Polyethylene glycol (PEG, Sigma, St. Louis, MO) was used as cross-linker for attachment of proteins of interest to the bead. The tip was first incubated with 10mM PEG for 5 minutes, followed by washing four times with distilled water, and then incubated with FN (0.25 mg/ml) or anti-α_5 antibody (1 mg/ml) for 5 minutes,

followed by rinsing four times with Phosphate-Buffered Saline (PBS) (1.05 mM KH_2P0_4, 155.17 mM NaCl, 2.96 mM Na_2HP0_4-$7H_20$). For all experiments, the AFM spring constants were assumed to be unchanged after protein labeling.

Nano-indentation protocol of AFM

Monitoring of biomechanical properties of single live VSMCs in real time was performed using a Bioscope II AFM system (Bruker, Santa Barbara, CA, USA) that was mounted on an IX81 OLYMPUS inverted microscope (Olympus Inc., NY, USA) (Fig. 2-1). All AFM measurements were conducted at room temperature in a 1% HEPES supplemented DMEM without antibiotics. The FN-coated spherical probe (Fig. 2-1D) was used to repeatedly indent and retract from the cell surface at 0.1Hz sampling frequency, 1000 nm ramp size. For each experiment, cells were randomly selected and indented at a site midway between the nucleus and cell margin. 60 force curves were collected over 10 minutes for a pre-drug period followed by 240 force curves over 40 minutes for the post-drug condition. To minimize the machine drift, after the probe was initially submerged in the cell bath, the AFM-microscope system was thermally and mechanically equilibrated for 1 hour. The analysis of force curves was processed by a custom analysis program written in MATLAB.

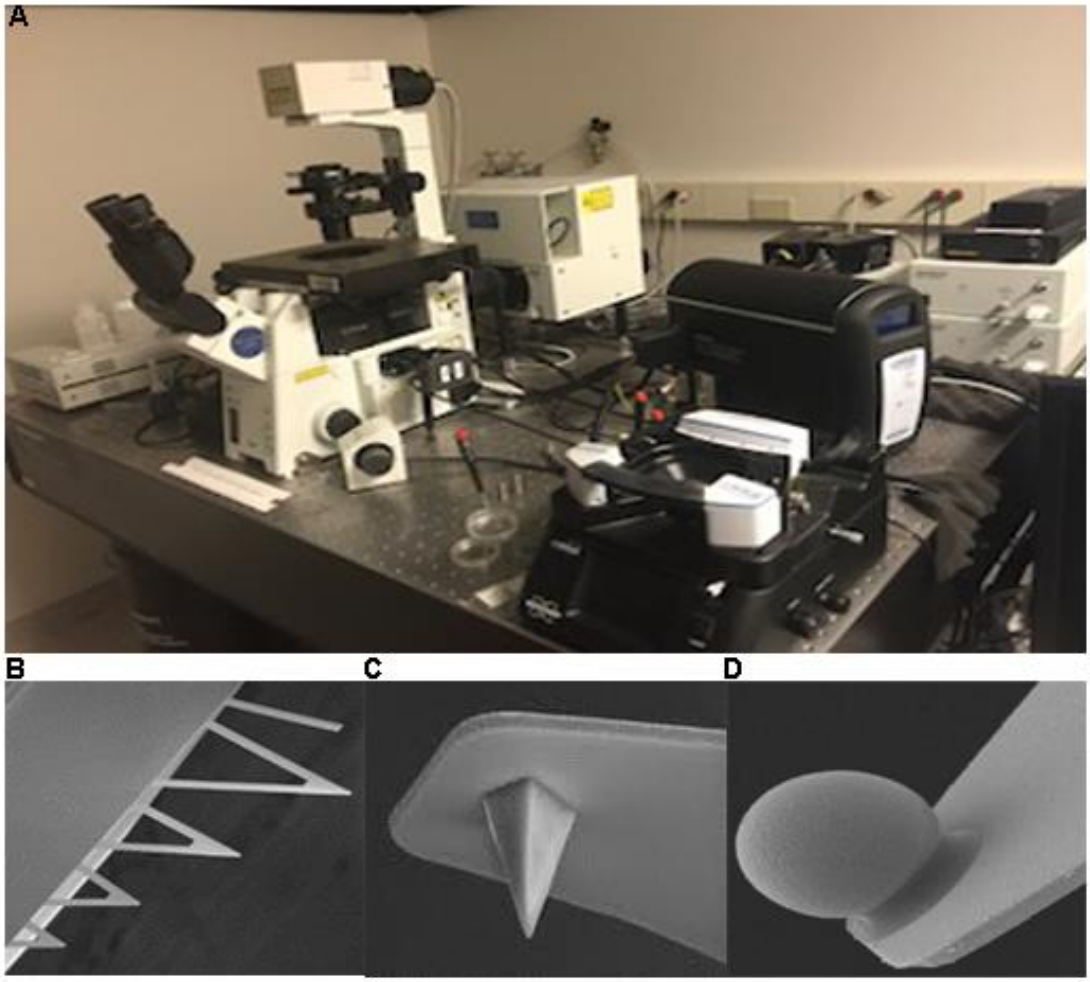

Figure 2-1. AFM system and AFM probe. (A) A Bioscope AFM system (Bruker, Corp. Santa Barbara, CA, USA) was mounted on a Fluoview confocal microscioe (Olympus, Thornwood, NY). (B) An AFM chip with 5 different probes. (C) An AFM probe used for contact mode scanning images and force volume images. (D) Spherical bead bond AFM probe used for measuring cell adhesion and cell stiffness.

Measurement of biomechanical properties with AFM

The stiffness measured with the nano-indentation protocol is an estimate of Young's modulus of elasticity (E-modulus) for the cell cortex, reflecting the cell's viscoelastic properties. A length of approximately 100-300nm of the AFM indentation curve, following the initial point of contact was fitted to a modified Hertz Model, which was used to assess the VSMC elasticity (Fig. 2-2B)

$$F = \frac{4}{3} \cdot \frac{\sqrt{rE}}{1 - v^2} \cdot \delta^{3/2}$$

Here, F is the force exerted by the AFM probe on the cell surface; *E* is the E-modulus; ν is Poisson ratio (assumed as 0.5); *r* is radius of spherical AFM tip; δ is indentation depth into the cell membrane. Rupture force, also referred to here as adhesion force between FN and integrin adhesion complexes, was determined from the retraction curves as the product of the rupture height and cantilever spring constant (Fig. 2-2C).

AFM contact mode imaging

To obtain a topographical cell image, the AFM tip was brought into contact with the cell surface and was placed in scanning mode to move it horizontally along the cell surface while applying a constant force (500 – 800 pN) to the cell. Scanned images were 100 μm × 100 μm at digital density of 512 pixels × 512 pixels. A stylus-type AFM probe (Fig. 2-1B, model MLCT-C, κ = 15pN nm^{-1}, Bruker, Santa Barbara, CA, USA) was used to perform the cell surface scanning at 0.15 Hz frequency at room temperature. Height and deflection image were collected with Bioscope software and analyzed using Nanoscope software.

AFM force volume imaging

Force volume was conducted to measure overall cell stiffness, scanning 100 μm × 100 μm at digital density of 128 pixels × 128 pixels. For each pixel, a stylus-type AFM probe was used to repeatedly indent and retract following previous nano-indentaion protocol at 0.1Hz. Deflection images were collected by Bioscope software and used to generate modulus image using Nanoscope software.

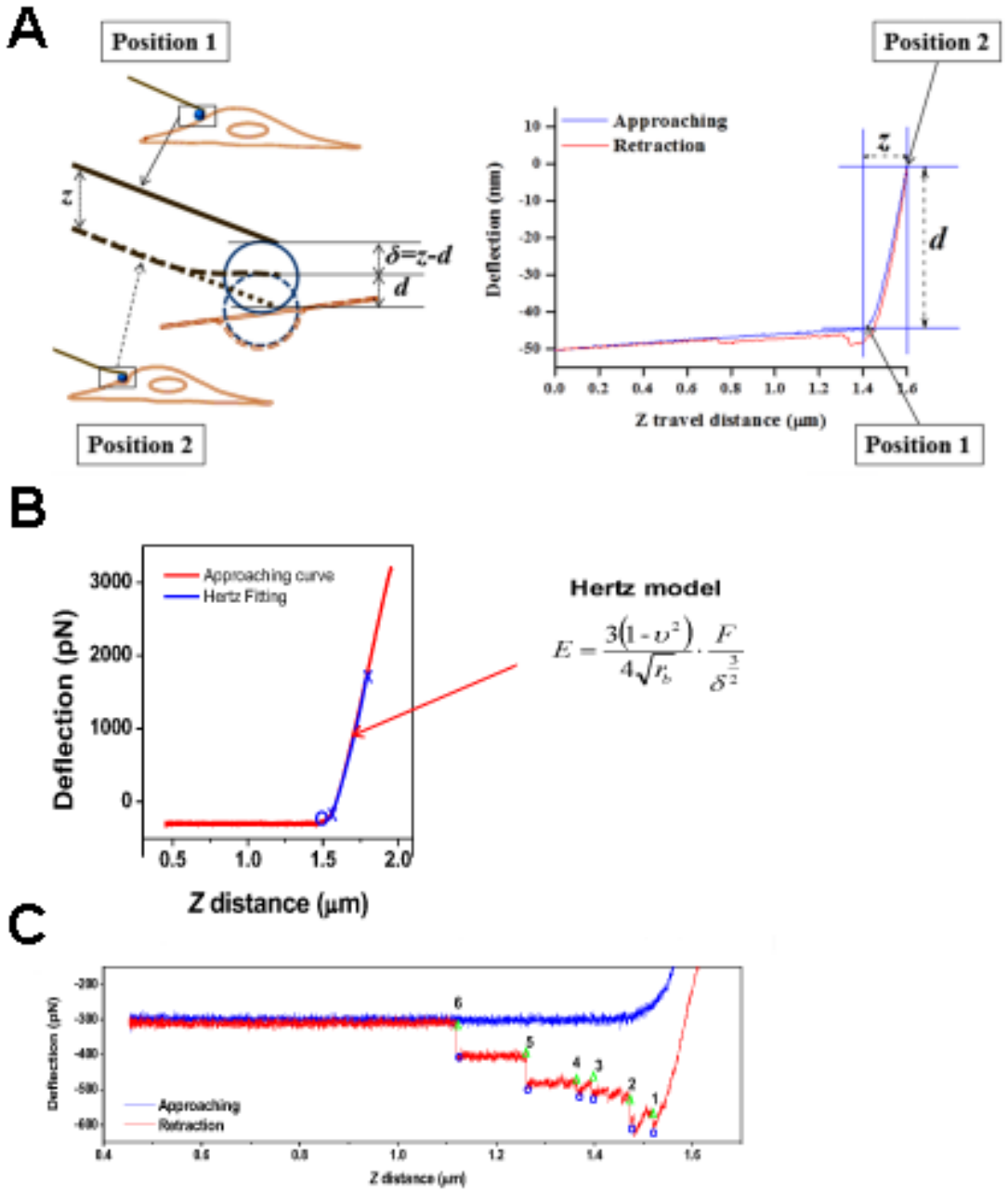

Figure 2-2. Illustration of the protocol used in an AFM experiment. (A) The FN coated AFM probe was cyclically interact with the VSMC membrane. The approach curve (blue) was fitted to Hertz model and used to estimate cell elasticity (B). (C) The adhesion data was collected from retraction curve. Adhesion was quantified as the number of ruptures that were counted as individual adhesion events and by adhesion force that was calculated by rupture height multiplied by cantilever spring constant.

Measurement of intracellular Calcium

Fluo-4 AM loading of VSMCs

Intracellular calcium was measured by imaging fluo-4 AM. Cells cultured on glass-bottomed tissue culture dishes (Corning incorporated, Corning, NY, USA) were washed with loading buffer (150 mM NaCl, 5 mM KCl, 1 mM MgCl, 10 mM glucose, and 20 mM HEPES, pH 7.4) twice and then incubated with 2.5 mM fluo 4-AM (Invitrogen Corp., Carlsbad, CA) in loading buffer (150 mM NaCl, 5 mM KCl, 1 mM MgCl, 10 mM glucose, and 20 mM HEPES, pH 7.4) supplemented with 2% BSA and 0.01 % Pluronic F-127 (BASF) for 25 minutes at room temperature on a rolling plate. Cells were then washed with loading buffer twice and then incubated at 30^{o}C in serum free DMEM for 20 minutes to allow the de-esterification.

BAPTA-AM Loading of VSMCs

Cells cultured on glass-bottomed tissue culture dishes were washed twice with loading buffer (150 mM NaCl, 5 mM KCl, 1 mM MgCl, 10mM glucose, and 20 mM HEPES, pH 7.4) and then incubated with 2.5 mM BAPTA-AM (Invitrogen, Carlsbad, CA) in loading buffer supplemented with 2% BSA and 0.01 % Pluronic F-127 (BASF) for 25 minutes at room temperature on a rolling plate agitator. Cells were then washed with loading buffer twice and then incubated at 30^{o}C in serum free DMEM for 20 minutes to allow the de-esterification.

Fluorescence imaging

To assess the correlation between cell stiffness and adhesion with intracellular calcium levels, we performed calcium imaging and made AFM measurements simultaneously. Calcium fluorescence images were collected continuously, starting at 20 seconds before the AFM pulling was applied, and ended 20 seconds after the pulling. Fluo-4-loaded VSMCs were visualized

using a confocal microscope (FV1000) equipped with a 488 nm laser, and the signal was collected at 510~550 nm ×60 oil immersion objective used for all imaging experiments. Fluo-4 images were analyzed using Fluoview software.

Cell staining for fluorescence immunocytochemistry and confocal microscopy

Prior to immunocytochemistry, VSMCs were serum-starved overnight. After treatment under different conditions (AII treated at 10^{-6}M for 30 minutes versus PBS exposure for 30 minutes, as a control), cells were washed with PBS three times followed by fixation with 2% paraformaldehyde for 30 minutes at room temperature. Cells were then quenched with glycine buffer (0.1mM glycine) three times for 10 minutes. After being washed, cells were incubated with primary antibody (1:100 dilution in labeling buffer: 150mM NaCl, 15mM $Na_3C_6H_5O_7$, 0.05% Triton X-100, 2% BSA) overnight at 4ºC. Cells were then washed six times with cold washing buffer (150mM NaCl, 15mM $Na_3C_6H_5O_7$, 0.05% Triton X-100), followed by incubation with Cy5-labeled secondary antibody (1:200 dilution in labeling buffer) and Alex 488-conjugated phalloidin (1:200 dilution in labeling buffer) for 2 hours at room temperature in a dark environment on a rolling plate. The cells were washed again by cold washing buffer and imaged with a confocal microscope using excitation wavelengths of 647nm and 488nm, respectively. A through-focus image set was collected for each cell with a z step interval of 0.2μm.

Statistical analysis

All data are reported as mean ± SEM. Statistical differences for comparisons of pre-drug controls and post-drug treatments were analyzed with paired t-test. ANOVA was used for between group analysis. All statistical

analyses were performed using open source software SCIDAVIS and StatPlus (AnalystSoft Inc., CA, USA). Differences were considered significant at $P \leq 0.05$.

RESULTS

Vascular Smooth Muscle Cell Characteristics

VSMCs were immuno-labeled for α-actin (anti-α-actin (red)) and stained with phalloidin (green), which is a widely accepted molecular marker for VSMC [105] in order to confirm the cells' identity. VSMCs exhibited the typical spindle-shaped morphology and displayed typical stress fibers visible after immuno-labeling (Fig. 2-3). Additional topology imaging of the VSMCs was performed using the AFM to obtain contact-mode deflection images of the VSMCs. Topology images revealed large, mostly parallel bands of cytoskeletal filaments (stress fibers) underlying the cell membrane surface (Fig. 2-3G). The topology images also showed the cell nucleus as the highest point of the cell above the culture substrate. The AFM was also used in force volume mode to measure stiffness at numerous randomly selected sites on the cell surface (Fig. 2-3E and F). The stiffness measurements showed that the nucleus had the lowest modulus of elasticity whereas the non-nuclear areas displayed higher elastic

modulus.

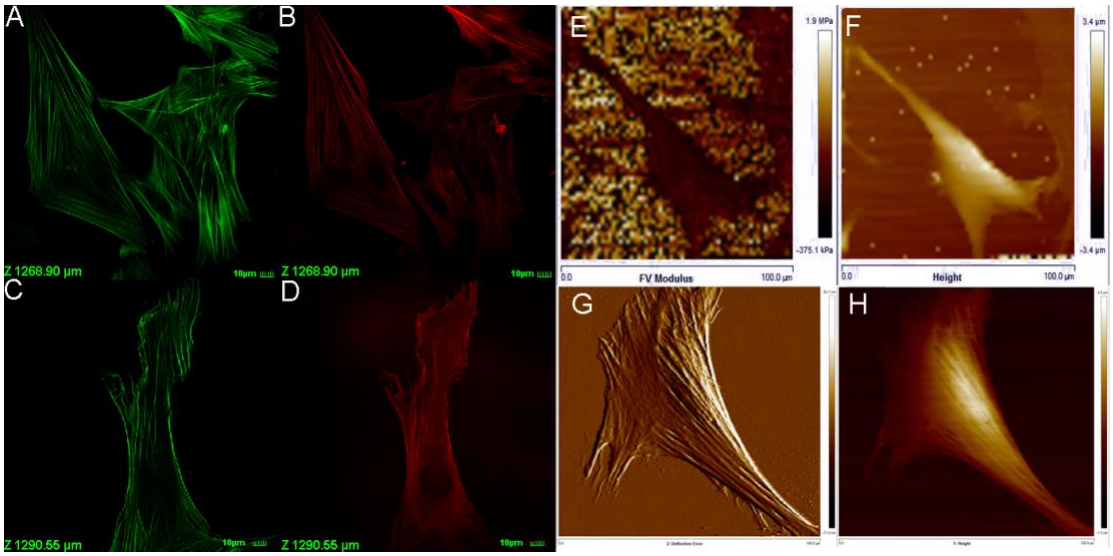

Figure 2-3. Images of cultured VSMCs. (A-D) Immunostaining of VSMCs with and α-actin (B and D, red) and staining of phalloidin (A and C, green). Cells exhibited spindle-shaped morphology and displayed numerous actin filaments and stress fibers (E and F). AFM images acquired in force volume mode showed softest site (lowest stiffness) on the cell surface and highest location was over the nucleus. Contact scanning images of deflection error (G) and cell height (H) on single cultured VSMC.

Force curves for analysis of FN-VSMC adhesion force

To measure the adhesion force between FN and cell surface integrins, FN-coated probes were applied to the surface of VSMC at randomly selected locations midway between the nucleus and cell margin (Fig. 2-4D). Two typical force curves are shown in Fig. 2-4. The blue trace line depicts the approach curve and the red trace line represents the retraction curve with the force plotted as a function of probe position. As the probe approaches the cell (point 1 to point 2), force remains at zero level. At the point that the probe contacts the cell surface (point 2), a resistance is encountered and a force increase is detected as the AFM cantilever is deflected. As indentation depth increases, the resistance force increases (point 2 to point 3) until the probe stops approaching and begins to retract. During probe retraction (red trace), the resistance force

declines (point 3 to point 4). In cases when there is no adhesion between FN and VSMC, the retraction curve resembles and overlays the approach curve (Fig. 2-4A). In contrast, if adhesions exist between the FN-coated AFM probe and the VSMC surface (Fig. 2-4B), pulling force increases during the retraction corresponding to adhesion strength and cantilever deflection is reversed. When the retraction force exceeds the strength of the adhesion, an abrupt force shift (point 5) is observed in the retraction curve, representing rupture of the adhesion between the AFM probe and cell. When all adhesions between the AFM probe and VSMC have been ruptured, the retraction curve again resembles the approach curve (point 6).

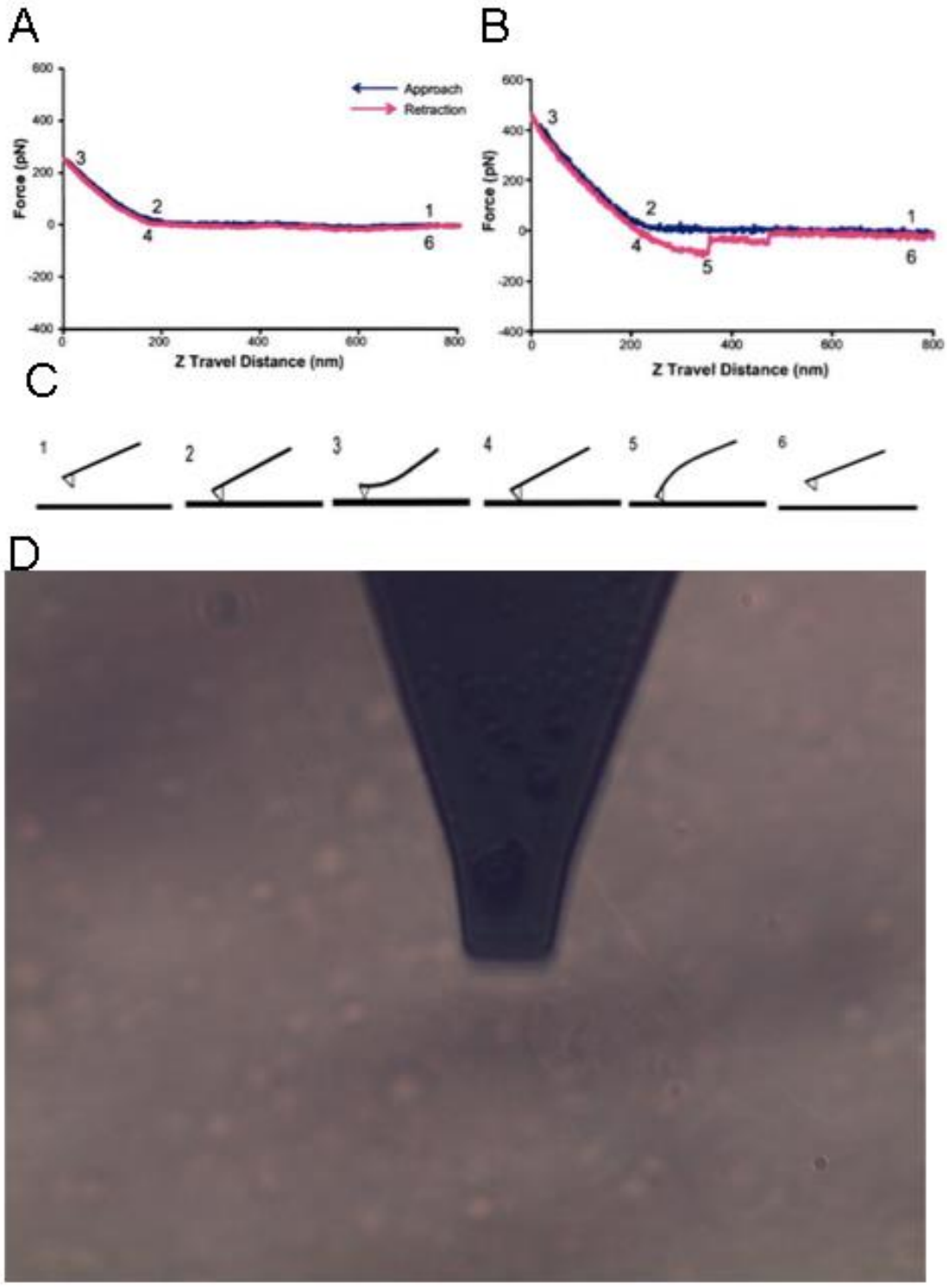

Figure 2-4. Typical force curves generated by AFM. (A) Retraction curve showing no adhesion between the AFM probe and the cell surface. (B) Retraction curve showing adhesion ruptures between the AFM probe and the cell surface. (C) A schematic of the AFM probe movement during the process of force curve generation. AFM fibronectin (FN)-coated probes were controlled to repeated approach and retract from VSMC surface at 0.1-Hz frequency. (D) Image of spherical AFM probe on VSMC.

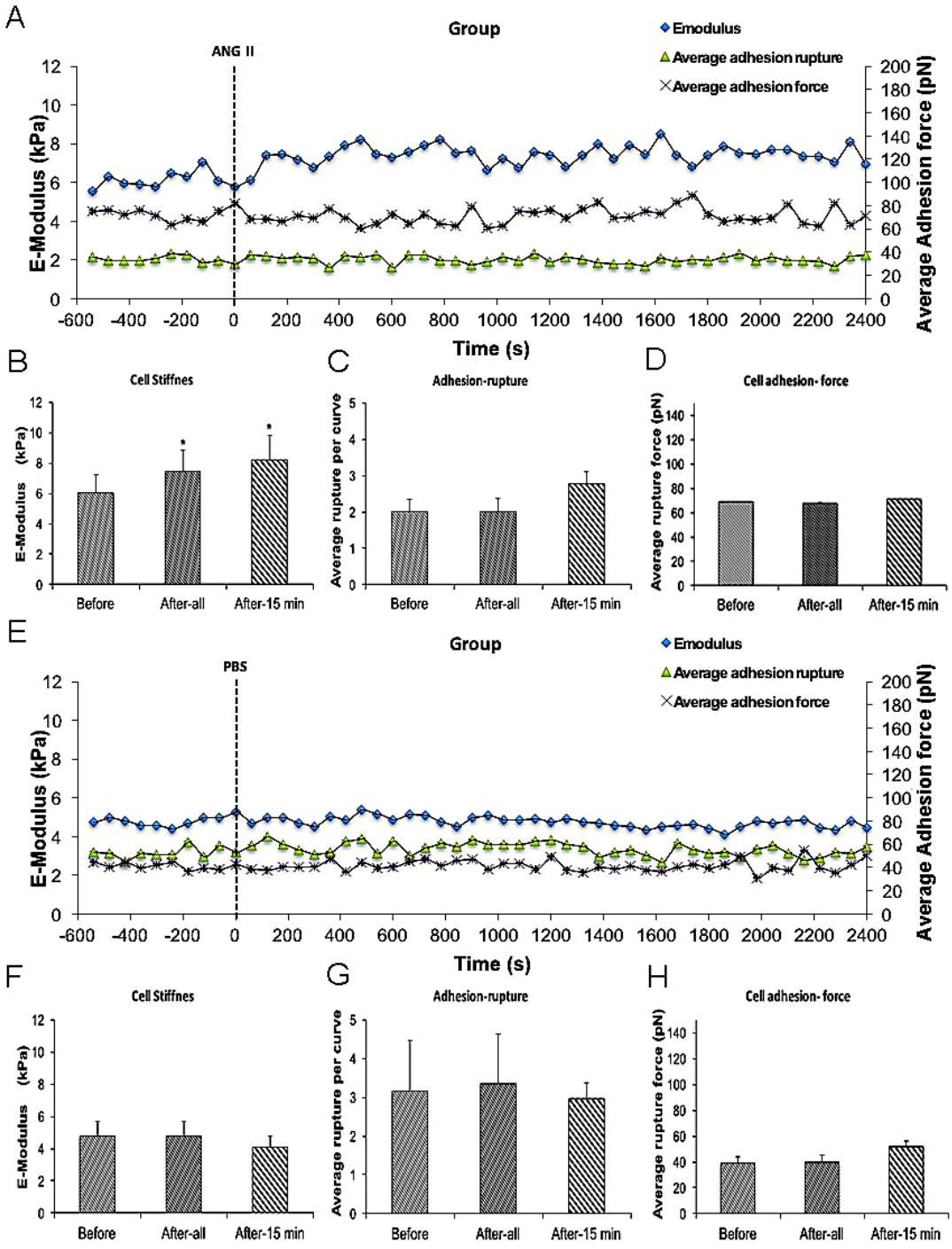

Figure 2-5. AII increased VSMCs stiffness but had no effect on cell adhesion to anti-α_5 antibody. Group average real-time recordings of cell stiffness (blue square), rupture events (green triangle), and rupture force (purple cross) for AII (n=8) treatment (A) and addition of PBS (n=10) (E). Average elastic modulus summed across all or 15 minutes of time points for the group of VSMCs before and after AII (10^{-6} M) treatment (B) (n=8, *P < 0.05) and PBS addition (F) (n=10, *P < 0.05). Average rupture numbers per curve summed across all or 15 minutes of time points for the group of VSMCs before and after addition of AII (C) (n=8, *P < 0.05) and PBS (G) (n=10, *P < 0.05). (D) Average rupture force summed across all or 15 minutes of time points for the group of VSMCs before

and after addition of AII (D) (n=8, *P < 0.05) and PBS (H) (n=10, *P<0.05). Data were collected at 0.1 Hz of indentation frequency and are presented as mean ± SEM.

Membrane expression of integrin α_5 following angiotensin II (AII) treatment

Previous work in our laboratory has shown that AII increases VSMCs stiffness as well as adhesion to FN [62, 66]. Specificity of FN binding to $\alpha_5\beta_1$-integrin on VSMCs was confirmed by demonstrating that adhesion was inhibited with function blocking antibodies to α_5 or β_1 integrins [88]. To determine whether the increased cell adhesion during AII treatment was due to enhanced membrane expression of integrin $\alpha5\beta1$, we used AFM probes coated with anti-α_5 antibody. We hypothesized that if AII was increasing the number of α_5 integrins on the cell surface, then adhesion to the antibody-coated probes would increase. In these experiments, 8 cells were treated with AII and of these 5 responded with the characteristic increase in cell stiffness whereas 3 of the cells did not respond. Only responsive cells were analyzed. The increase in cell stiffness (blue circle) was gradual after AII exposure and reached a plateau after approximately 15 minutes, which is consistent with previous reports from our laboratory (Fig. 2-5A). Before treatment, average cell stiffness was 6.04 ± 0.26 kPa, and which increased to 7.47 ± 0.21 kPa after AII representing a statistically significant increase by 24% (Fig. 2-5B). As a control, VSMCs were treated with PBS which showed no effect on cell stiffness (Fig. 2-5E and F).

Cell adhesion was analyzed in the AII responsive cells and was quantified as the number of ruptures per curve (Fig. 2-5A, green triangles) and the total rupture force (Fig. 2-5A, purple crosses). After AII treatment, cell

adhesion to anti-α_5 antibody, measured as rupture number per curve (Fig. 2-5C), was not significantly increased. In addition, rupture force showed no observable increase with AII (Fig. 2-5D). PBS-treated cells also showed no effect on average rupture number per curve or total rupture force (Fig. 2-5E, G, and H).

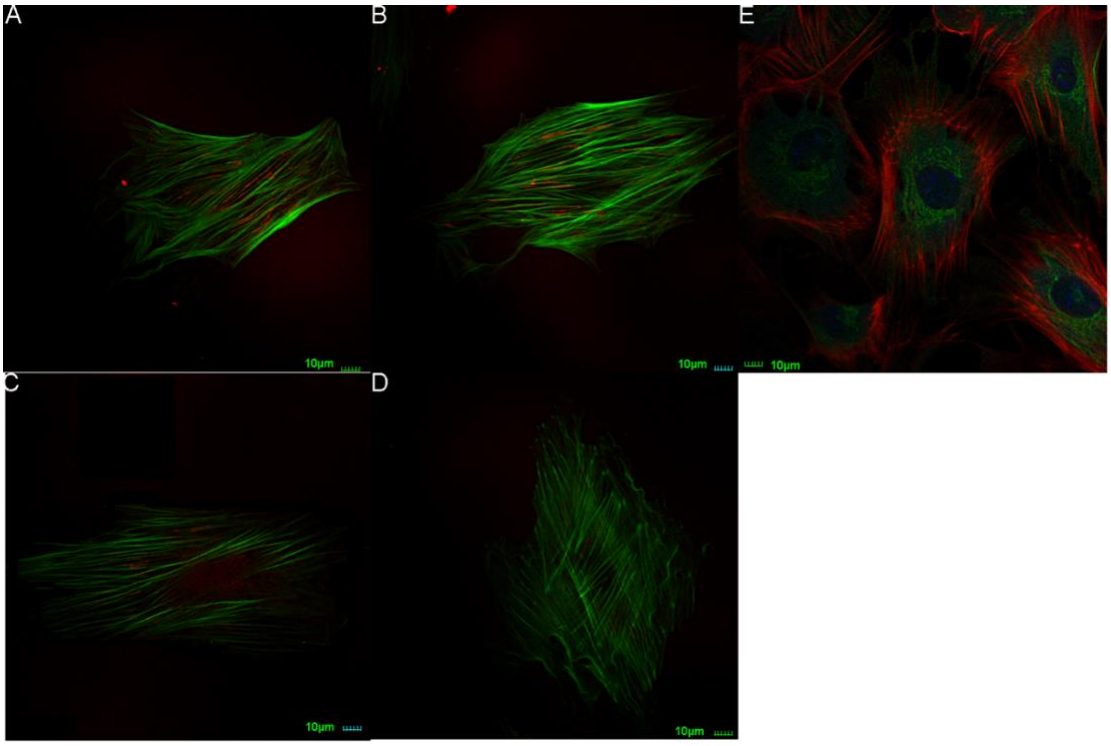

Figure 2-6. AII has no effect on expression of integrin α_5 in VSMCs. (A-D) Immunostaining of integrin α_5 (red) and labeling with phalloidin (green) on VSMCs before treatment (A), after addition of AII (10^{-6} M) (B) and PBS (C). (D) is negative control without anti-integrin α_5 as primary antibody. (E) Immunostaining of nucleus (blue), Angiotensin II Type I receptor (ATIR, green), and phalloidin (red). Scale bars represent 10 μm.

As a further test to confirm a lack of change in expression of integrin α_5, we also performed immunostaining of α_5 on VSMCs. Cells were co-labelled with phalloidin to visualize cell stress fibers. Immunofluorescence confocal microscopy showed that α_5 integrin was diffusely distributed on the apical

surface of VSMCs (Fig. 2-6A). After treatment with AII, there were no observable changes of α_5 distribution on the cell surface or intensity of labelling (Fig. 2-6B). As control group, PBS treatment also had no effect on α_5 distribution or labelling intensity (Fig. 2-6C). In Fig. 2-6E, immunostaining of angiotensin receptor subtype 1 (AT_1R) (green) was also performed on VSMCs together with phalloidin (red). AT_1R shows widely distributed on apical surface of cells. Collectively, these data suggest that AII-induced increases in VSMCs adhesion to FN does not result from enhanced membrane expression of integrin α_5. Rather, these data are consistent with an effect of AII to increase integrin activation.

Effect of KCl treatment on VSMC stiffness and adhesion to FN

AII is known to act on the AT1R and to cause increases in intracellular Ca^{2+} ($[Ca^{2+}]_i$) in VSMCs [106, 107]. To test the hypothesis that $[Ca^{2+}]_i$ was playing a role in the enhanced adhesion to FN and increase in cell stiffness we utilized KCl (60mM). KCl is a non-receptor agonist which increases levels of $[Ca^{2+}]_i$ secondary to cell depolarization. In these experiments, FN (0.25mg/ml) coated AFM probes were used to measure cell stiffness and adhesion response to KCl. Before treatment, average cell stiffness was 7.64 $\pm$ 1.65 kPa, and application of KCl induced a rapid transient and significant increase in cell stiffness to 18.87 $\pm$ 4.39 kPa (Fig. 2-7A, blue circle) representing a 142% increase (Fig. 2-7B, blue square) (Fig. 2-7C). During the period when cell stiffness was transiently elevated we observed that cell adhesion to FN was also transiently increased. The increase in adhesion was apparent as a significant increase (129%) in the numbers of ruptures per curve (Fig. 2-7A and

D, green triangle) and increase in total adhesion force (177%) (Fig. 2-7A and E, purple cross).

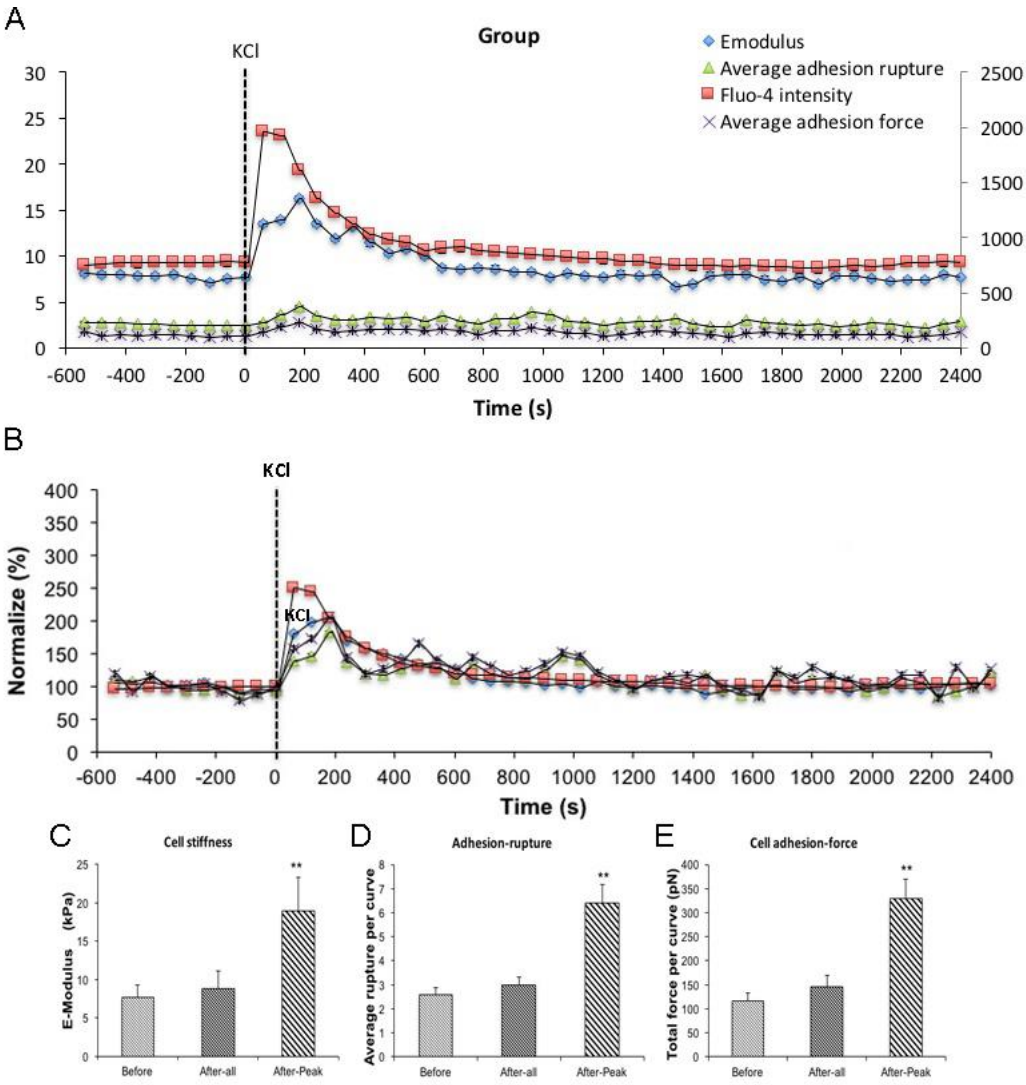

Figure 2-7. KCl transiently enhanced cell stiffness and cell adhesion to FN as well as intracellular calcium level ($[Ca^{2+}]_i$). (A) Group average real-time recordings of $[Ca^{2+}]_i$ (red), cell stiffness (blue), rupture events (green), and rupture force (purple) before and after addition of KCl (n=10). (B) Group recordings of $[Ca^{2+}]_i$ (red), cell stiffness (blue), rupture events (green), and rupture force (purple) normalized to average summed all time points of before-treatment (n=10). (C) Average elastic modulus summed across all of time points and peak response for the group of VSMCs before and after addition of KCl (60 mM) (n=10, **P < 0.01). (D) Average rupture numbers per curve summed across all of time points and peak response for the group of VSMCs before and after addition of KCl (n=10, **P < 0.01). (E) Average rupture force summed across all of time points and peak response for the group of VSMCs before and after addition of KCl (n=10, **P < 0.01). Data were collected at 0.1 Hz of indentation frequency and are presented as mean ± SEM.

Involvement of $[Ca^{2+}]_i$ as a mediator of changes in cell stiffness and adhesion

To confirm Ca^{2+} was changing following KCl treatment, VSMCs were loaded with the fluorescent calcium indicator fluo-4. $[Ca^{2+}]_i$ measurements were obtained while simultaneously performing AFM to measure cell stiffness and adhesion to FN. KCl induced a transient increase in levels of $[Ca^{2+}]_i$ that correlated with the increased cell stiffness, as well as the increases in adhesion ruptures and total adhesion force (Fig.2-7A and B, red square). It was noted that $[Ca^{2+}]_i$ levels reached maximum levels immediately preceding the changes in cell stiffness and cell adhesion. These data suggest that calcium-related signaling is linked to the observed changes of cell stiffness and adhesion. As a further test of the involvement of $[Ca^{2+}]_i$ as a mediator of the observed changes in stiffness and adhesion, VSMCs were treated with the calcium chelator, BAPTA. As shown in Fig. 2-8A, BAPTA-treated groups of cells showed slightly decreased stiffness, however this reduction was not statistically significant compared to cells of PBS-treated groups. However, average adhesion ruptures significantly declined 24% ($p<0.01$) in BAPTA-loaded cells (Fig. 2-8B) compared to the control group. BAPTA treated cells also showed significant reduction in total adhesion force, which decreased 25% (Fig. 2-8C). To confirm an effect of BAPTA on $[Ca^{2+}]_i$, experiments were performed on fluo-4 loaded VSMCs. BAPTA-loaded cells showed significantly decreasing $[Ca^{2+}]_i$ compared to the PBS-treated control group at p level of 0.01 (Fig. 2-8D). Thus, these data further suggest $[Ca^{2+}]_i$ plays a role in altering integrin adhesion.

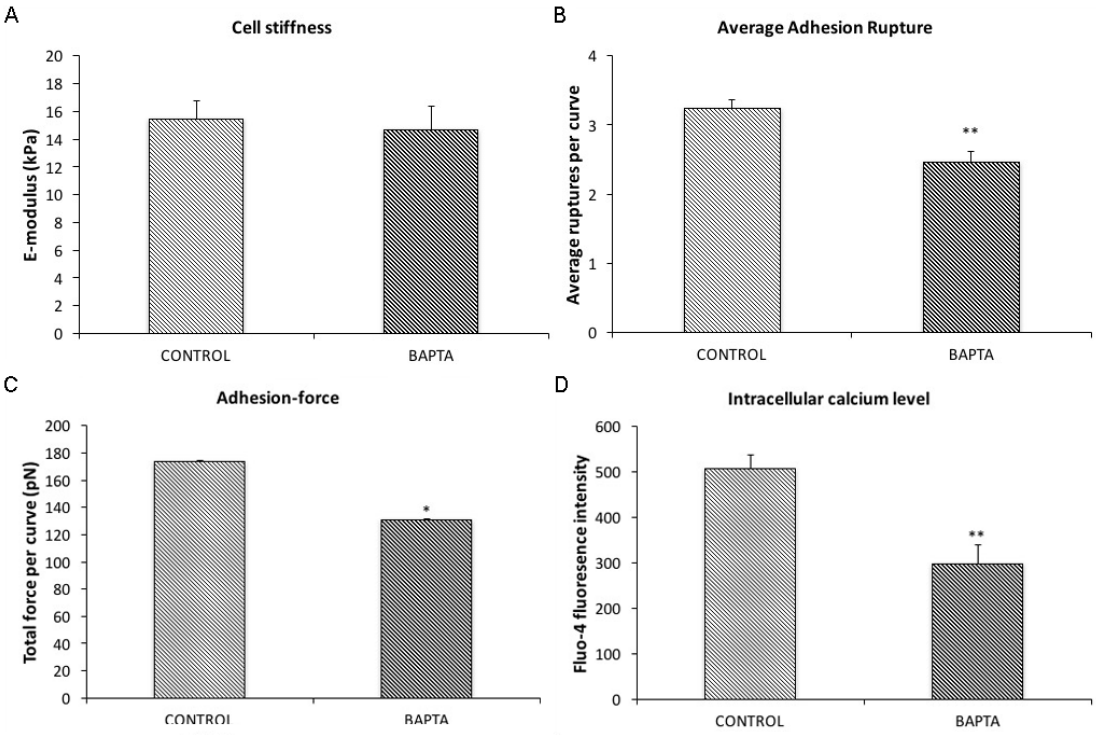

Figure 2-8. BAPTA treatment decreased cell adhesion to FN but has no effect on cell stiffness. (A) Average elastic modulus for the group of VSMCs with and without BAPTA-treatment (10^{-6} M). (B) Average rupture events per curve for the group of VSMCs with and without BAPTA treatment (n=10, **P < 0.01). (C) Average rupture for the group of VSMCs with and without addition of BAPTA (n=10, **P < 0.01). (D) Level of $[Ca^{2+}]_I$ for the group of VSMCs with and without addition of BAPTA (n=10, **P < 0.01). Data were collected on randomly selected 5 cells, each cell was recorded 2 minutes at 0.1 Hz of indentation frequency. Data are presented as mean ± SEM.

Effects of inhibition of myosin light chain kinase

$[Ca^{2+}]_i$ elevation leads to VSMC contraction through activation of myosin light chain kinase (MLCK) via calcium-calmodulin complex [108]. To further investigate the role of $[Ca^{2+}]_i$ in cell stiffness and adhesion to FN, VSMCs were treated with ML7, a myosin light chain kinase inhibitor prior to treatment with KCl. $[Ca^{2+}]_i$ was also measured using fluo-4. After ML-7 treatment, VSMCs E-modulus was decreased to 35% when it was normalized to pre-drug period (Fig. 2-9B, blue circle) measured during the last 10 minutes of ML-7 treatment period compared to pre-drug period in cell stiffness (Fig. 2-9C) but there was no effect

on adhesion ruptures (Fig. 2-9D) or adhesion force (Fig. 2-9E). $[Ca^{2+}]_i$ was not significantly increased by ML-7 and then back to base. Compared to pre-drug condition (Fig. 2-10A), ML-7 treated VSMC exhibited a loss of stress fibers or the large bands of actin cytoskeletal filaments underlying the cell membrane (Fig. 2-10B). Topographic images of the VSMCs also revealed cell height decreased following ML-7 (FIG. 2-10C and D). Following application of KCl to the ML7-treated cells (Fig. 2-9A, blue circle) there were no observable changes on the effect of KCl on stiffness or adhesion as either rupture numbers or adhesion force. Therefore, these results further support the involvement of $[Ca^{2+}]_i$ in cortical cell stiffness and adhesion to FN and further suggest that increased cell stiffness and adhesion was not dependent on actin-myosin interaction.

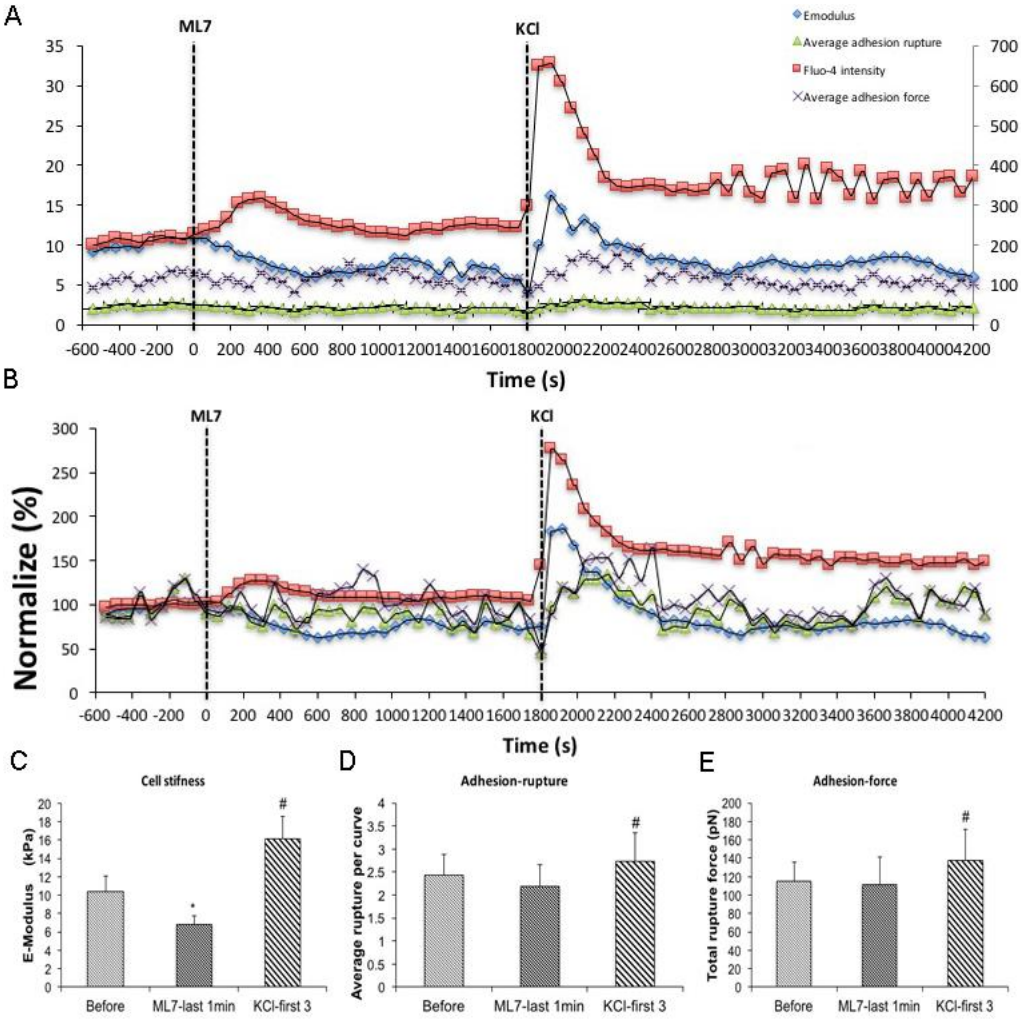

Figure 2-9. With pre-treatment of ML-7, KCl elevated cell stiffness, cell adhesion to FN as well as level of $[Ca^{2+}]_i$. (A) Group average real-time recordings of $[Ca^{2+}]_i$ (red), cell stiffness (blue), rupture events (green), and rupture force (purple) before and after addition of ML-7 and KCl (n=10). (B) Group recordings of $[Ca^{2+}]_i$ (red), cell stiffness (blue), rupture events (green), and rupture force (purple) normalized to average summed all time points without treatment (n=10). (C) Average elastic modulus summed across all time points for the group of VSMCs before treatment, time points of 15 minutes of ML-7 (15 μm) and first 3 time points after addition of KCl (60 mM) (n=10, *P < 0.05 compared to no-treatment, #P < 0.05 compared to ML-7). (D) Average rupture numbers per curve summed across all time points for the group of VSMCs before treatment, time points of 15 minutes of ML-7 (15 μm) and first 3 time points of after addition of KCl (60 mM) (n=10, *P < 0.05 compared to no-treatment, #P < 0.05 compared to ML-7). (E) Average rupture force summed across all of time points for the group of VSMCs before treatment, time points of 15 minutes of ML-7 (15 mm) and first 3 time points of after addition of KCl (60 mM) (n=10, *P < 0.05 compared to no-treatment, #P < 0.05 compared to ML-7). Data were collected at 0.1 Hz of indentation frequency and are presented as mean ± SEM.

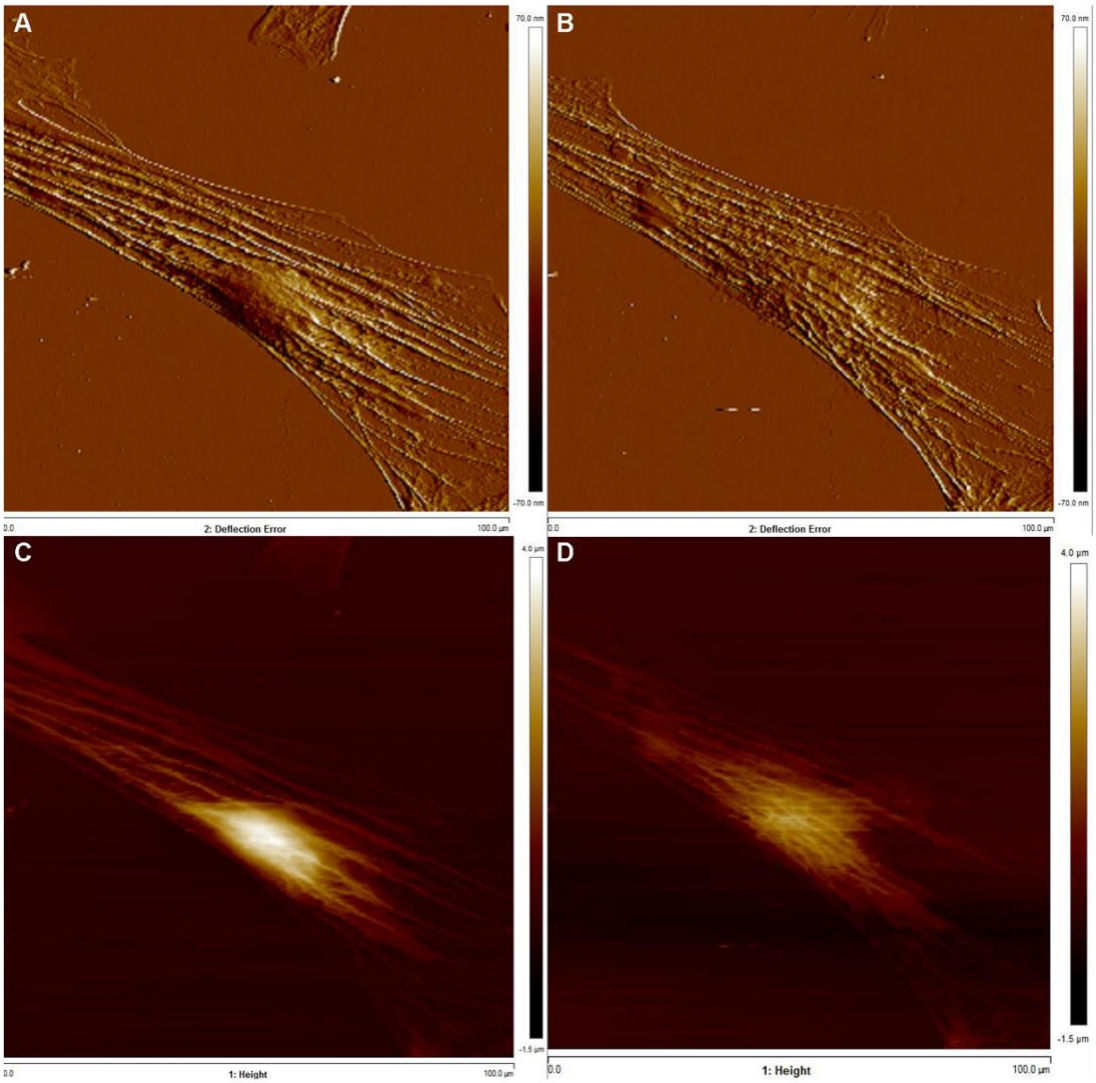

Figure 2-10. Contact-mode images of VSMCs with ML7. (A-B) Images of deflection error of single cultured VSMC of before treatment (A) and after ML7 treatment (B). (C-D) Height images of single cultured VSMC of before treatment (C) and after addition of ML7 (D).

DISCUSSION

Previously, Hong et al. [66] have shown in VSMCs that vasoactive agonists induced coordinated changes in cell elasticity and integrin-mediated cell adhesion. That specifically, vasoconstrictors increase VSMC elastic modulus and simultaneously enhance cell adhesion whereas vasodilators have the opposite effect [66]. In this study, our results confirm that the regulation of ECM adhesion and the contractile activation state of vascular smooth muscle are dynamically linked. The results also demonstrate this coordinated link is synchronized with $[Ca^{2+}]_i$. We tested the hypothesis that the contractile activation of VSMCs with elevated $[Ca^{2+}]_i$ would enhance adhesion to the ECM protein FN and that the change in adhesive behavior would be coordinated with increases in VSMC cortical stiffness. The increase in cortical stiffness was assumed to act as an indication of changes in the state of VSMC contractile activation. As a corollary to this, we postulated that lower $[Ca^{2+}]_i$ would produce opposite results characterized by decreased adhesion to FN and a parallel reduction in VSMC cortical stiffness.

Real-time fluo-4 confocal image combined with AFM was used to record cell stiffness and adhesion to FN along with $[Ca^{2+}]_i$. We confirmed that increases in cell stiffness and adhesion to FN occurred in the presence of a rapid but transiently increase $[Ca^{2+}]_i$ that was induced by KCl. The results indicated a high degree of correlation between the increase in $[Ca^{2+}]_i$ and cell stiffness and adhesion. As contraction of VSMC follows from increased $[Ca^{2+}]_i$, we inhibited the contractile interaction of actin and myosin with ML7. By preventing contractile filament interaction, we sought to determine whether the

changes in cortical stiffness and cell adhesion were linked as a downstream event of the contractile process or occurred as a set parallel events coordinated with contraction through changes in $[Ca^{2+}]_{i.}$ The results of these experiments indicated that the changes in cell stiffness and adhesion persisted in the presence of the inhibition of MLCK supporting the interpretation that that coordination with contraction is likely regulated by a pathway parallel to but not downstream of contraction. We then sought to lower $[Ca^{2+}]_i$ by Incubation with the calcium chelator BAPTA. We reasoned that lowering $[Ca^{2+}]_i$ would not only inhibit contractile filament interaction but would also inhibit any parallel pathway dependent on $[Ca^{2+}]_{i.}$ The results confirmed that lowering $[Ca^{2+}]_i$ reduced cell stiffness and cellular adhesion to FN providing additional support for the conclusion that there is a parallel pathway activated upstream of the contractile pathway.

The cytoskeleton of VSMC provides a structural framework that determines cell shape/morphology and mechanical properties. These characteristics are determined by both dynamic actomyosin interactions as well as by the capacity of the actin cytoskeleton to rapidly depolymerize and repolymerize [109]. In this study, the protocol used to measure VSMC stiffness resulted in cell surface indentation by the AFM probe of ~100-300 nm. Thus, the changes in measured cell elasticity should be viewed as largely representing the cortical stiffness of the cell's stress fibers underlying the cell membrane. It is well established that the cortical cytoskeleton network physically connects to deeper cytoskeletal elements within the cytosol as well as to adhesion zones that regulate adhesion to the ECM [110-112]. Cortical stiffness is mechanically determined by cellular cortex elasticity and cortex

tension, which is believed to be mostly governed by myosin-generated contractility [113, 114]. The changes in VSMC stiffness we observed in the presence of inhibition of MLCK are consistent with interpreting the alterations in stiffness as changes in the polymerization state of the cortical cytoskeleton.

Phenylephrine (PE) is another vasoconstrictor that has also been reported to induce cortical stiffening in VSMC without affecting focal adhesion size via FAK-ERK signaling. These data support a correlation between cellular cortical stiffness and cellular contractile state [115]. Together with the present result that pretreatment of ML-7 did not blunt KCl effects on cell stiffness and adhesion (Fig. 2-9), these data further indicate calcium exerts its effect via calcium-related signaling pathway other than downstream of actin myosin interactions. Given previous findings from Hong et al. that cytoskeletal remodeling occurs in VMSCs following AII treatment [62], calcium appears to exert its effect on cell stiffness through changes in actin polymerization. Calcium-calmodulin-dependent protein kinase II (CaMKII) has been reported to regulate actin cytoskeletal assembly [116], which might suggest a possible mechanism of calcium effect. However, more experiments will be needed to demonstrate underlying mechanisms of involving cytoskeletal remodeling and calcium.

The responsiveness of VSMCs used in this study to AII confirmed the retention of characteristics expected of a contractile phenotype. This is important because cultured VSMCs carried in culture over many passages exhibit a transition from a contractile phenotype to a synthetic phenotype [117, 118]. In our studies, only primary cell cultures were used without passage to minimize these phenotypic changes. Despite these precautions, it is not

possible to completely prevent phenotypic shifting and this may account for why only 80% of the cells we studied were AII responsive (data not shown).

VSMCs cellular adhesion to FN was assessed by measuring the force required to produce rupture events between the FN coated AFM probe adhering to the VSMC. This was quantified as number of rupture events per force curve and the force that break adhesion bonds formed between VSMCs and FN on the AFM probe. An increase in detectable rupture events and/or force was interpreted as a change in integrin-mediated cell adhesion. Another possibility is that an increase in the number of rupture events induced by an agonist might be related to mechanical wrinkling or ruffling of the cell membrane that decreases the cell surface area such that integrin density per unit membrane area would be augmented and impact the number of detected adhesions. However, pretreatment of VSMC with ML-7 to prevent any cell contraction, did not change KCl-induced adhesion to FN (Fig. 2-9). This evidence argues against a membrane contraction-induced change in integrin density. Also, in previous studies by Hong et al. [66] increases in adhesion force were detected following AII suggested that the increase in adhesion was accompanied by changes in the molecular connections of the integrin to cytoskeletal components. This also argues against argument of the change in membrane area.

Previous studies have shown that adhesion events and corresponding rupture forces measured by FN-decorated AFM probes are specific interactions between FN and $\alpha_5\beta_1$ integrins [88, 96]. Thus, in this study, changes in adhesion is also likely $\alpha_5\beta_1$ integrin-dependent. It has been demonstrated in migratory cells that integrin trafficking to and from the membrane can regulate

focal adhesion size through assembly and/or disassembly resulting in spatial integrin redistribution of membrane integrins [119]. In our study, to assess whether there was a possible change of integrin expression on membrane that could contribute to an increase in adhesion via the number of detectable rupture events, we coated spherical AFM probe with anti-α_5 antibody. The anti-α_5 antibody that was selected shows affinity for both active and inactive forms of the α_5 integrin. We reasoned that if the AII was increasing the amount of integrin on the membrane then the anti-α_5 antibody would show an increase in adhesion events following AII. Our results demonstrated that there was no change in adhesion to the anti-α_5 antibody coated AFM probe following AII treatment (Fig. 2-5). These data support the interpretation that AII-induced changed in adhesion to FN was occurring through a process of integrin activation rather than integrin turnover.

In summary, our studies show coordination of VSMC cortical stiffness and cell adhesion following contractile activation that is synchronized with changes in $[Ca^{2+}]_i$. ML-7 results further confirmed cell stiffness was related to contractile state since inhibition of MLCK reduced resting cell stiffness, but ML-7 did not inhibit KCl induced coordination of enhanced cortical stiffness and adhesion to FN. These observations suggest that calcium-induced cell stiffness and adhesion is parallel to the contractile activation pathway and not downstream of actin and myosin interaction. This information is an important advance in our understanding of the mechanisms underlying coordination of cell stiffness and adhesion to ECM. We propose this coordination is essential to provide the mechanical efficiency and ability of the VSMCs to appropriately adapt itself to mechanical changes brought about through intracellular

contractile activation and likely extracellular changes in applied force. Increased vascular stiffness is a significant feature of aging and occurs in cardiovascular disease, such as hypertension and atherosclerosis [30, 31]. Further investigations into the underlying mechanisms governing both the cellular mechanics and adhesion of VSMC may lead to possible therapeutic targets that through the link between these pathways and vascular disease.

CHAPTER III

INTEGRIN ADHESION RESPONSE TO VERTCIAL OSCILLATIONS

ABSTRACT

Physical coupling of vascular smooth muscle cells (VSMCs) to extracellular matrix proteins (ECM) by integrins is required for efficient mechanotransduction. Integrin adhesion receptors are essential for normal vascular function and defective integrin signaling at focal adhesions is associated with cardiovascular disease. Vascular smooth muscle cells (VSMCs) are continuously exposed to dynamically changing mechanical forces related to changes in arterial pressure, pulse pressure and shear forces. However, little is known about focal adhesion and integrin behavior in the presence of dynamic changes in the forces acting at the focal adhesion. The overall purpose of the study was to gain insight into focal adhesion and integrin behavior by using a combination of mathematical modelling supported and informed by biological experiments. Mathematical models are a useful tool for gaining quantitative insights into the behavior of complex dynamic systems through their ability to predict biological behavior in response to change. In this study, we collaborated with applied mathematicians to test a model simulation of how integrin adhesions respond to changes in mechanical force applied as a vertical oscillatory force. Model simulations predicted that integrin adhesions would exhibit ‘bistability’ depending on the level of the applied mechanical load. The bistability would present as a change in the point at which all integrin bonds

rupture depending upon whether load is increasing from a completely bound state or decreasing beginning with an unbound state. We used atomic force microcopy (AFM) to experimentally mimic the applied vertical oscillation in force that were simulated in the model to attempt to verify this model prediction. The AFM probe was operated to cyclically approach and retract a fibronectin (FN)-coated spherical AFM probe from the cell surface. Two conditions were compared, one in which the probe was pre-bound to the cell to form an established focal adhesion and the second in which there was no prebinding of the probe to the cell. Retraction amplitudes were varied by setting different retraction ramp sizes. The results indicated that at retractions from the cell surface of 1000 nm and shorter integrin adhesion to FN dominated over integrin adhesion ruptures as the small retraction amplitudes were not sufficient to detach the integrins from the FN on the AFM probe. At larger amplitude displacements, for example 2000 nm retraction ramp size, there was sufficient probe separation from the cell surface to cause complete rupture of all integrin bonds with each cycle regardless of initial integrin bonds formed on contact. This was true for both the pre-bound and non-prebound conditions. However, for intermediate amplitude retraction distances, for example, 1200 nm ramp size, pre-bound and non-pre-bound results differed. In the prebound condition the integrin adhesions were more resistant to disruption and adhesion prevailed whereas in the non-pre-bound condition integrin adhesion ruptures showed dominance. In conclusion, our experimental data support the existence of “bistability’ for integrin adhesions that is dependent on initial conditions of adhesion and thus support the model predictions. The bistable nature of adhesion behavior in the presence of dynamic oscillations suggest that integrin

signaling could be quite different depending on the balance between integrin adhesion vs. adhesion rupture.

INTRODUCTION

Many vascular functions are associated with mechanical forces including regulation of blood pressure, tissue blood flow, capillary pressure, peripheral resistance, permeability, leukocyte adherence, and vascular remodeling [120-122]. As the major cellular component of arterial vessels, vascular smooth muscle cells (VSMCs) are constantly exposed to mechanical stimuli in their environment and have evolved several mechanisms to sense and respond to these cues. The process that vascular cells are to sense mechanical forces and change them into intracellular signals to elicit specific cellular response is known as mechanotransduction, and is linked to changes in the cell contractile state as well as gene expression, growth and cell phenotype [123-125]. Existing data supports the idea that mechanotransduction is linked to a variety of cell surface proteins of which, integrins appear to play a central role [125, 126]. Integrins provide a direct link from the extracellular matrix (ECM) environment to the cytoskeleton and can bi-directionally transmit physical forces and play a role in outside-in and inside-out signaling. Upon binding with ECM proteins, integrins cluster together and recruit through their intracellular domains numerous scaffolding and signaling proteins to form the focal adhesion complex [17, 127].

The involvement of integrins in mechanotransuction has been extensively studied for both ‘outside-in’ pathways and ‘inside-out’ pathways. From ECM to the cell, it has been shown that integrins act as sensors of mechanical properties generated within the local microenvironment and convey

this information to the cell. It is well accepted that ECM-cell interactions are dynamic processes. In this regard, vascular smooth muscle cells (VSMCs) are exposed to continuously changing mechanical forces related to changes in arterial pressure, pulse pressure and shear forces. However, little is known about focal adhesion and integrin behavior in the presence of dynamic changes in the forces acting at the focal adhesion. This information is important to understand how cell signaling and ultimately cell and vascular behavior will be influenced. The overall purpose of the study was to gain insight into focal adhesion and integrin behavior by using a combination of mathematical modelling supported and informed by biological experiments. Mathematical models provide a useful approach for gaining quantitative insights into the behavior of complex dynamic systems through their ability to predict biological behavior in response to change. To date there very few published mathematical models of integrin-related cellular process [128, 129], and there are no studies using mathematical models to try to understand integrin behavior to dynamically changing forces.

In this study, we combined our biological expertise for study of integrin behavior in VSMCs with the mathematical modeling expertise of colleagues. A mathematical model of integrin adhesion behavior was developed that simulated the behavior of integrin adhesions in response to oscillating mechanical stretching of different magnitudes. In this study, we used atomic force microcopy (AFM) to experimentally mimic the applied vertical oscillation in force that were simulated in the model to attempt to test model predictions. The model simulations predicted that integrin adhesion would vary dependent on applied force amplitude and initial conditions of integrin adhesion to the

ECM. We directly tested these predictions by using a fibronectin (FN)-coated AFM probe that could be controlled to interact with the cell to mimic the model simulations.

METHODS

Mathematical simulation model

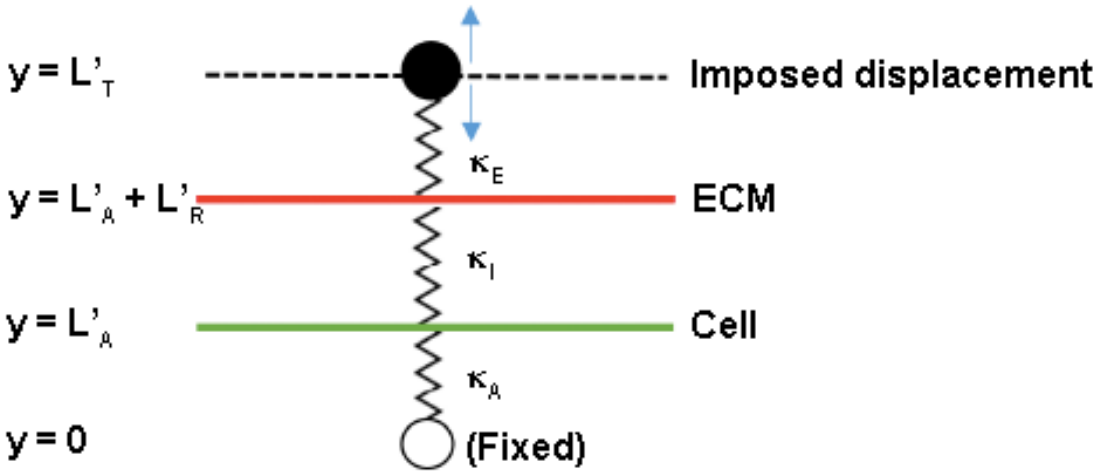

Figure 3-1. Illustration of 3-spring model for vertical oscillation. The 3-spring model for vertical deformation of linear elastic materials representing the cell, bound integrins, and the ECM. The cell, integrins, and ECM springs have rest length L_A, L_R, and L_E and deformed length L'_A, L'_R, and L'_E respectively. The total fraction of bound integrins is given by $B(t) = \int_{-\infty}^{\infty} \hat{b}\,(\hat{x}, \hat{t})\, d\hat{x}$, and the integrin spring strength is proportional to this quality. For predictions of integrin adhesion behavior, the vertical amplitude was cyclically varied through a series of different amplitudes representing low, intermediate and high stretches.

Figure 3-1 illustrates a schematic model of an integrin focal adhesion interacting with the extracellular matrix (ECM). In this 3-spring model, the vascular smooth muscle cell (VSMC), integrins and ECM are each represented as linear springs with the spring constants κ_A, κ_I, κ_E, respectively. The spring constants κ_A, κ_I, κ_E represent the cell stiffness, collective stiffness of bound integrins (acting in parallel) and ECM stiffness, respectively. The resting lengths of the springs are represented by L_A, L_R, and L_E and force induced deformed

lengths are represented as L'$_A$, L'$_R$, and L'$_E$, respectively. The total fraction of bound integrins is given by the integral: $B(t) = \int_{-\infty}^{\infty} \hat{b}\,(\hat{x},\hat{t})\,d\hat{x}$, and it is determined by integrins (χ) distribution $\hat{b}(\hat{x},\hat{t})$, and distance $d\hat{x}$ between the integrin and the ECM. The integrin-bound fraction takes on a value between 0 and 1 with 0 representing no bound integrins and 1 representing all integrins fully bound. The total number of bound integrins at any point in time is given as ρB. According to Hooke's law, the vertical adhesive force is given by $\hat{F}_y(\hat{t}) = \rho\hat{\lambda}_b B\hat{L}$, in which $\hat{\lambda}_b$ is integrin spring constant, and $\hat{L}$ is integrin extended distance.

Using this model, a vertical oscillatory displacement was applied by varying the y-coordinate, L'$_T$, to the location of the ECM. This is represented by the following equation:

$$L'_T = \frac{L_T + A}{2} + A(-1)^{[2\omega t+1]}\,(\frac{1}{2} + 2\omega t - [2\omega t + 1])$$

where $L_T/2$ is minimum height of the oscillating layer (i.e. when the approach of the ECM to the cell is complete), A is the magnitude of the oscillation, and ω is the frequency of oscillation. This model generates a trace of the time courses of the fraction of bound integrins, B, and vertical adhesion forces as we vary the amplitude A in the wave equation. This model was developed in collaboration with Dr. Bindi Brook, Dr. Reubin O'Dea and Linda Irons at the University of Nottingham. These model predictions were then experimentally tested on isolated aortic VSMCs using an atomic force microscope (AFM). The AFM probe was labelled with ECM and the AFM used to control and mimic the oscillation pattern used in the model. The methods for the biological experiments follow.

Materials and reagents used

For all cell isolations, dithioerythriotol, papain, collagenase, soybean trypsin inhibitor, and elastase were purchased from Sigma (St. Louis, MO, USA). For studies described human plasma fibronectin (FN), Bovine Serum Albumin (BSA), and PEG were purchased from Sigma (St. Louis, MO, USA). For studies using atomic force microscopy (AFM) a bioscope II AFM system (Bruker, Santa Barabara, CA, USA) was mounted on an IX81 OLYMPUS inverted microscope (Olympus Inc., Thorwood, NY). AFM data were collected and analyzed using Nanoscope (Bruker, Santa Barbara, CA, USA) and Matlab (MathWorks, Natick, MA, USA) software.

Cell preparation

Animal and Tissue preparation

Male Sprague-Dawley rats (200 g-300 g) were used in this study and were maintained in accordance with the protocol of the Guide for the Care and Use of Laboratory Animals (NIH 83-23, revised 1996). The animal protocol was reviewed and approved by the Laboratory Animal Use Committee (ACUC) of the University of Missouri. Animals were housed individually in a 12:12 light-dark cycle and had free access to food and water. Tissue samples of the thoracic aorta were isolated as described in previous work [130]. Briefly, rats were anesthetized by intraperitoneal injection of pentobarbital sodium (Lundbeck, Inc., Deerfield, IL, USA) at 0.1 g/kg. A surgical plane of anesthesia was confirmed by observing no spinal reflex to a toe pinch. The rat chest was opened and the thoracic aorta from the descending thoracic aorta to the diaphragm excised (~ 1-2 cm) placed quickly to in cold (4^{o}C) Ringer's buffer (composed of 145 mM NaCl, 4.7 mM KCl, 2.0 mM $CaCl_2(2H_20)$, 1.0 mM

$MgSO_4(7H_20)$, 1.2 mM $NaH_2PO_4(H_2O)$, 0.02 mM EDTA, 3.0 mM MOPS, 5 mM Glucose, 2.0 mM Pyruvic Acid). Vessel and cell isolation were performed in solution based on Ringer's buffer. Anesthetized rats were euthanized by intracardial injection of saturated KCl solution (3 ml). The aorta tissue was moved on a silicone rubber pad in a bath of cold Ringer's buffer and cleaned of fatty tissue. After draining of blood by changing buffer solution, the adventitial layer was carefully isolated and removed with help of a stereomicroscope. The aorta was then cut open longitudinally, and then endothelium was gently scrapped off with finely-toothed forceps and aortic tissue minced into approximately 1 mm^2 squares. The tissue pieces were then placed into culture dish (35 cm^2) with Ringer's buffer in room temperature and subsequently processed to isolate vascular smooth muscle cells (VSMCs).

VSMCs isolation and culture

VSMCs were enzymatically isolated using previously described methods with minor modification [104]. Briefly, thoracic aortic pieces were transferred to a glass culture tube (10 ml) that contained 1 ml of the first cell dissociation solution consisting of Ringer's solution, 27 U/ml of papain and 1mg/ml dithioerythriotol. The segments were incubated at 37 ^oC for 45 minutes without agitation. At the end of this interval, the first cell dissociation solution was carefully decanted and replaced with 1 ml of second cell dissociation solution consisting of Ringer's solution with 0.5 U/ml collagenase, 75 U/ml elastase, and 1 mg/ml soybean trypsin inhibitor. The segments were further incubated for 30 minutes at 37 ^oC. At the end of the incubation period, the dissociation solution was carefully decanted and washed twice by adding 1 ml Hank's solution, followed by 1 ml serum free DMEM/F12 (Invitrogen, Carlsbad, CA, USA) The

vessels segments were triturated by pipetting 2 ml DMEM for approximately 20-30 times to disperse individual cells from the tissue. The solution containing the dispersed VSMCs was then transferred into 60 mm tissue culture dishes (Corning incorporated, Corning, NY, USA), and maintained under culture conditions in a humidified incubator with 5% CO_2, at 37^oC in DMEM supplemented with 20% fetal bovine serum (FBS, ATLANTA Biologicals, Laurenceville, GA, USA), 10 mM HEPES (Sigma, St. Louis, MO, USA), 1 mM sodium pyruvate, 2 mM L-glutamine, 100 U/ml penicillin, and 100 g/ml streptomycin. After 48 hours' incubation, the culture medium was changed to DMEM/F12 supplemented with 10% FBS. The cells used in all experiments were maintained under these conditions for 5-10 days without passage. Prior to an experiment the VSMCs were serum-starved overnight.

Force spectroscopy measurement

Bio-functionalized AFM probes

A 5 μm diameter glass bead (Structure Probe Inc., West Ghester, PA, USA) was glued on the tip of an AFM probe (MLCT-O10, Bruker Corp., Santa Barbara, CA, USA) and then coated with FN using the protocol previously used in our Laboratory [88]. Briefly, before gluing the glass bead to the cantilever tip, each cantilever was calibrated before a given experiment using thermal noise amplitude analysis. Cantilevers were then cleaned first by rinsing in 100% ethanol twice followed by rinsing in acetone for 3 times. The cantilever was dipped in glue (Progressive Epoxy Polymers Inc., USA) and then brought into contact with a glass bead mixture in solution that had been smeared on a glass slide. After bead attachment AFM probes were stored for 48 hours to allow bead glue to cure. The AFM probe with attached bead was then processed to

bio-coat the bead tip. Polyethylene glycol (PEG, Sigma, St. Louis, MO) was used as cross-linker for attachment of proteins of interest to the bead. The tip was first incubated with 10 mM PEG for 5 minutes, followed by washing four times with distilled water, and then incubated with FN (1 mg/ml) for 5 minutes, followed by rinsing four times with phosphate-buffered saline (PBS) (1.05 mM KH_2P0_4, 155.17 mM NaCl, 2.96 mM Na_2HP0_4-$7H_20$). For all experiments, the AFM spring constants were assumed to be unchanged after protein labeling.

Vertical oscillation protocol of AFM

Monitoring of biomechanical properties of single live VSMCs in real time was performed using a Bioscope II AFM system that was mounted on an IX81 OLYMPUS inverted microscope. All AFM measurements were conducted at room temperature in a 1% HEPES supplemented DMEM without antibiotics. To minimize drift, after the probe was initially submerged in the cell bath and the whole system was thermo-equilibrated for 1 hour. After thermal equilibration, the FN-coated spherical probe (Fig. 2-1D) was used to repeatedly indent and retract from the cell surface at 0.1Hz sampling frequency. To determine the effect of withdrawal ramp size on the adhesion characteristics between FN and the VSMC, ramp sizes were varied throughout a range from 200 nm to 2000 nm. Force curves were obtained for ramp increases at steps of 200 nm over the entire range. Two types of protocols were followed for each ramp size. The first is a Prebind protocol in which the AFM probe was allowed to attach onto the VSMC and the second a Non-prebind protocol in which the probe was not pre-attached to the VSMC.

(1) Pre-Bind Protocol: An AFM probe with a FN-coated bead attached was brought into contact with the VSMC surface. The probe with bead was maintained in

contact with the cell membrane for 20 minutes to allow formation of a stable focal adhesions. After 20 minutes, the oscillation experiments were performed.

(2) Non-Prebind Protocol: An AFM probe with a FN-coated bead attached was brought into contact with the VSMC surface. The AFM was set to immediately begin oscillating by performing approach and retraction cycles after it engaged the cell membrane. In this protocol, there was no delay period of contact with the cell to allow formation of a focal adhesion.

For each experiment, cells were randomly selected and indented on the nucleus site, and 60 force curves were collected over 10 minutes. All of AFM measurements were conducted at room temperature in serum-free medium. The analysis of force curves was processed by a custom analysis program written in MATLAB.

AFM measurements

Measurements of pulling force, bead displacement, and distance between ECM and the cell were collected and calculated from continuous force curves. The pulling force was generated by the bending of the AFM cantilever and was calculated according to Hooke's law as follows:

$$F = d \times k$$

where F is force (in pN), d is cantilever deflection (in nm), and k is the cantilever spring constant (in pN/nm). Bead displacements were recorded for 10 minutes and reconstructed by Matlab. Distance between ECM and the cell was calculated by total ramp size minus displacement of initial contact point.

Statistical analysis

Experimental data of non-prebind and prebind condition were compared in statistical difference by two-sample Kolmogorv-Simirnov test. Differences were considered significant at $P \leq 0.05$.

RESULTS

In the simulation model described in the methods, the cell, integrins, and ECM were represented by linear springs and a vertical oscillatory displacement was imposed with amplitude A. In experiments, amplitude was applied through ramp size of AFM from 200 nm to 2000 nm.

Model predictions versus experimental results

1. Low amplitude displacement simulation and experimental results

1.1 Simulation model

Low amplitude oscillations were simulated as $A = 2$, that the bound fraction stays high as there is insufficient separation distance between the ECM and the cell to create full rupture of bound integrins. For the non-pre-bind condition (Fig. 3-2A red line), when the ECM layer approached the cell membrane, integrin bonds were formed over time and reached an equilibrium or bound saturation point relative to the duration of contact. Given the low amplitude oscillations of displacement there are only small amounts of integrin ruptures for each cycle. In the pre-bind condition (Fig. 3-2A blue line), a maximum number of integrin bonds form in advance of imposing the oscillatory displacements. Similar to the non-pre-bind condition, the majority of integrins remain attached and a small amount of oscillatory rupture fraction was observed. Thus, the adhesion behavior to applied oscillatory force under pre-bind condition and non-pre-bind condition were equivalent and adhesion dominates over adhesion rupture.

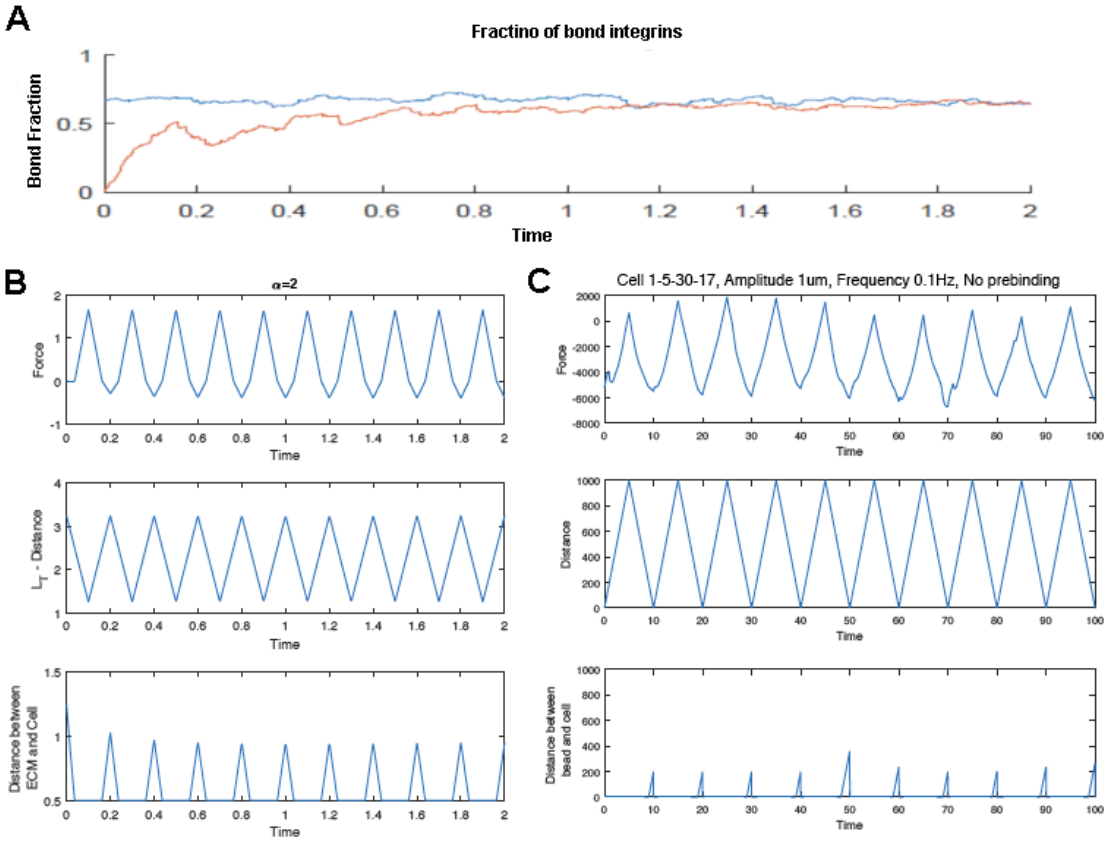

Figure 3-2. Low amplitude oscillatory simulation and experimental results. (A) Integrin bound fraction in simulation at low amplitude (A = 2) stretching. (B) For low amplitude (A = 2) in the simulation model, result of force, ECM displacement, and distance between ECM and cell are displayed. (C) At experimental amplitude 1000 nm, result of force, bead movement, and distance between bead and cell. Most of integrins maintain adhesion and the low amplitude oscillations cause only a small fraction of integrin ruptures in both simulation model and experimental results. In other words, integrin adhesion dominates over integrin rupture in the presence of low amplitude stretching because imposed stretch is insufficient to induce rupture.

1.2 Comparison of experimental data to model predictions

AFM experiments on VSMCs were performed at displacement ramp sizes of 200 nm – 1000 nm to test the mathematical model predictions for low amplitude oscillations. Figure 3-2C presents a representative data set collected at ramp size of 1000 nm and an oscillation frequency of 0.1 Hz on a thoracic VSMC. These experiments were performed without an AFM pre-attachment of

the FN coated AFM probe to the VSMC (non-prebind condition). The distance between FN-coated bead and the cell slightly increased with applied oscillatory displacement and applied force, which is consistent with the mathematical simulation (Fig. 3-2B). Upon contacting the VSMC with FN, integrin adhesions formed and saturated over the duration of the oscillating contact period. As the distance between bead and cell was only slightly increased, most of the integrin bonds survived and did not rupture. Thus, the experimental data at 1000 nm supported this mathematical model in low amplitude oscillatory force ($A = 2$).

2. High amplitude displacement simulation and experimental results

2.1 Simulation model

High amplitude oscillations were simulated as $A = 4$, and in this condition, applied oscillational displacement and forces are sufficiently large that there is full adhesion detachment at each cycle of the oscillation. In other words, all integrin adhesions with the ECM rupture. As illustrated in Figure 3-3A, in both zero (red line) and saturated (blue line) initial condition, applied oscillatory force was large enough to completely break the ECM and the rupture fraction dominated for the cell and integrin bonds. Due to the large displacement amplitude, the adhesion predicted behavior was the same for the pre-bind condition and non-pre-bind conditions.

2.2 Comparison of experimental results to model predictions

To mimic the high amplitude displacement simulation, AFM experiments on VSMCs were performed at ramp size of 2000 nm to test the mathematical model predictions. Figure 3-3C showed a representative data set that was collected at ramp frequency of 0.1 Hz on a VSMC without forming saturated integrin bonds (non-prebind). As depicted in Figure 3-3C, distance between FN-

coated bead and the cell was augmented by increased displacement and applied force. We found that a 2000 nm ramp sized was large enough to completely break all bonds formed between the FN-coated AFM probe and the VSMC. These data are entirely consistent with and supportive of the predictions of the mathematical model (Fig. 3-3B).

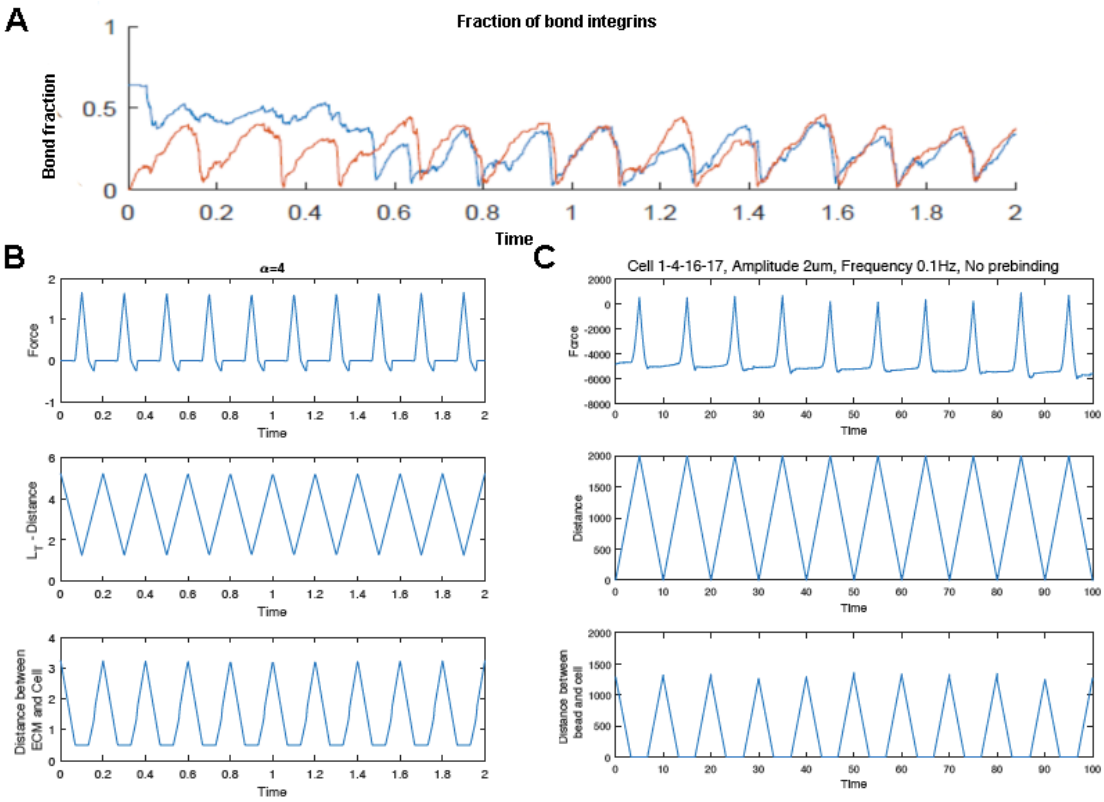

Figure 3-3. High amplitude oscillatory simulation and experimental results. (A) Integrin-bound fraction in simulation model for high amplitude (A = 4) stretches. (B) For high amplitude (A = 4) in the simulation model, result of force, ECM moved distance, and distance between ECM and the cell are displayed. (C) At experimental amplitude 2000 nm, result of force, bead movement, and distance between bead and cell were determined. High amplitude stretches cause all integrin adhesions to rupture for each cycle of stretch in both simulation model and experimental results. Stretch exceeds adhesive potential of the bound integrin fraction and adhesion rupture dominates over adhesion.

3. Intermediate amplitude displacement simulation and experimental results

3.1 Simulation model

For intermediate displacement, a value of $A = 2.475$ was selected. Under intermediate displacement the model predicted two possible outcomes that were dependent on the initial binding conditions (Fig. 3-4A). For the non-prebind condition where there are zero-initial existing adhesions (Fig. 3-4A, red), there is full rupture of all adhesions because the separation distance between the cell and ECM was sufficiently large to rupture the individual adhesions. However, under the pre-bound condition (Fig. 3-4A, blue), the integrin adhesions showed resilience in the presence of the displacement and there was adhesion survival. Thus, integrin adhesions exhibited two types of behavior in response to intermediate level displacement, which we defined as 'bistability'. As shown in Figure 3-4B, at the same applied oscillatory force, ECM-cell separation distance was larger in non-pre-bound (blue) condition than in the pre-bound condition.

3.2 Comparison of experimental results to model predictions

To replicate the intermediate amplitude displacement simulation, AFM experiments on VSMCs were performed at ramp size of 1200 nm to test the mathematical model predictions. Representative results of an experiment representing the non-prebind initial condition (Fig. 3-4C) and pre-bind initial condition (Fig. 3-4D) display force and bead-cell separation, respectively. For the non-prebind condition (Fig. 3-4C), adhesion ruptures were observed indicating that the displacement was sufficient to disrupt the integrin adhesions. However, adhesion ruptures were not observed in the pre-bind condition (Fig. 3-4D). Furthermore, cells in pre-bind condition showed shorter separation distance of bead-cells than those in non-prebind condition. These experimental results closely match the predictions resulting from the mathematical model

(Fig. 3-4B). Thus, experimental results provided evidence supporting 'bistability' behavior of integrin adhesions.

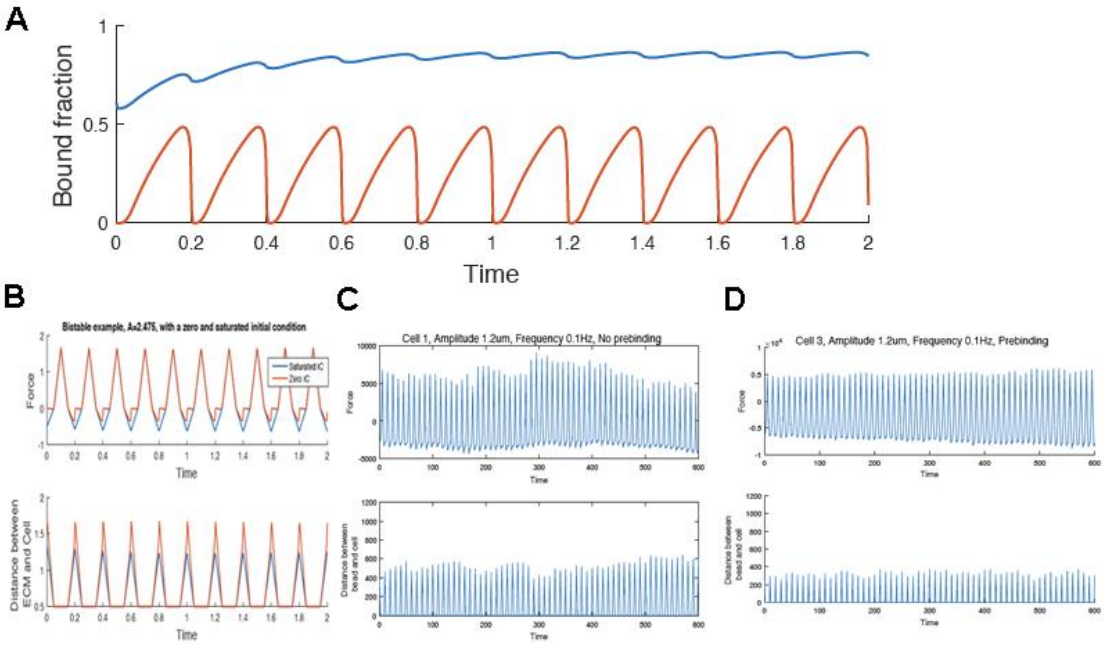

Figure 3-4. Intermediate amplitude oscillatory results for simulation and experimental studies demonstrate 'bistability'. (A) Integrin bound fraction in simulation model of intermediate amplitude (A = 2.475). (B) For intermediate amplitude (A = 2.475) in simulation model, result of force, ECM moved distance, and distance between ECM and cell are displayed. (C) At experimental studies an amplitude of 12000 nm represented intermediate stretch, result of force, bead movement, and distance between bead and cell are displayed. For intermediate amplitude oscillations, the dominance of Integrin adhesion versus integrin rupture has different outcomes based on initial conditions of the integrin ECM interaction. Cells of non-prebind condition that prevent formation of an established focal adhesion showed larger cell-bead separation distance on stretching than did cells that were pre-bound to the ECM and had established focal adhesions. This revealed a transition state at which rupture would begin to dominate over adhesion.

DISCUSSION

In this study, we provide experimental data to test a mathematical model of integrin binding to the ECM in response to vertical oscillations of displacement distance between the ECM and the cell. Model simulations were designed based on two initial conditions. The first condition was what is referred to as non-prebind in which there exist zero-integrin ECM bonds under the initial

condition. This was achieved by starting oscillations immediately after the AFM probe was engaged to cell surface. The second condition is referred to as pre-bound in which the ECM and cell have had sufficient time to interact to allow all available integrins to bind to the ECM creating a saturated-integrin bond initial condition. To experimentally replicate the non-prebind condition, we used a FN-coated AFM to approach and retract cyclically from the cell surface. By comparison, to mimic the pre-bind condition we engaged the FN coated with the VSMC for a 20-minute period to allow adhesion to the FN and formation of a focal adhesion before initiating cyclic retraction/approach. Previous studies from our laboratory have shown that 20 minutes of contact with and FN-coated AFM probe allows consistent and stable focal adhesion formation between the FN-conjugated bead and cell surface integrins which was confirmed by the presence of α_5-integrins and actin clustered around the circumference of the bead [88, 127].

Based on the predictions of the simulation model, it can be seen that integrin adhesion to the ECM is determined by the presence of initial integrin bonds and amplitude of applied oscillatory force/displacement. Simulations with both low and high amplitude oscillatory force/displacement, cell integrin adhesion to ECM predicted similar behavior in both pre-saturated initial condition and non-prebind zero-formed integrin bonds condition. Integrin adhesion dominated over ruptures in low amplitude simulation while high amplitude induced complete break of integrin bonds and rupture dominated adhesion. In contrast, for intermediate amplitude simulation, integrin adhesion demonstrated ‘bistability’ with adhesion behavior showing two possible outcomes that depended on the initial condition. Under pre-bind conditions

adhesion dominated over adhesion rupture whereas under non-prebind conditions adhesion rupture began to be exhibited. These simulations suggested that prebinding placed the integrins in an enhanced state of stability.

Experimental classification of high/low/intermediate adhesion states

To experimentally test the proposed mathematical model, we first had to determine the range of displacements required to mimic the high, low and intermediate adhesion sates. In the simulation model, the classification of the adhesion states is determined by the bound fraction of integrins and simulation results are expressed by the bound fraction of integrins that remains in response to varying the oscillation amplitude. By comparison, the bound fraction of integrins is a model-derived parameter and could not be measured experimentally with the AFM. Instead, to approximate the integrin bound fraction, we used the AFM to directly measure and apply nanoscale force to ECM-induced focal adhesion sites. We could also closely approximate bound integrin fraction and integrin adhesion state by measuring the bead-cell separation distance, which is also predicted by the simulation model. Therefore, the peaks in the bead-cell distance, which represents the maximum separation between bead and cell during each cycle, was used as measurement of the adhesion state. For comparison of model simulation and experimental data, we plotted the maximum, mean and minimum cell-bead separation for different amplitude oscillations of the simulations model in Figure 3-5A. A high separation (seen for high amplitude oscillations) indicates the full rupture state, whereas the low separation (seen for low amplitude oscillations) shows there some remaining adhesions. Simulations show there is a small window of bi-stability for intermediate values of A (e.g. A=2.425, 2.475). For lower amplitude

oscillations (<2.4), the separation between cell and ECM approaches zero. The peak bead-cell separation distance of experimental data for full range of amplitudes showed in Figure 3-5B. Compared with simulation model, biological data showed similar distribution patter that transit point showed around ramp sizes of 1000 nm and 1400 nm.

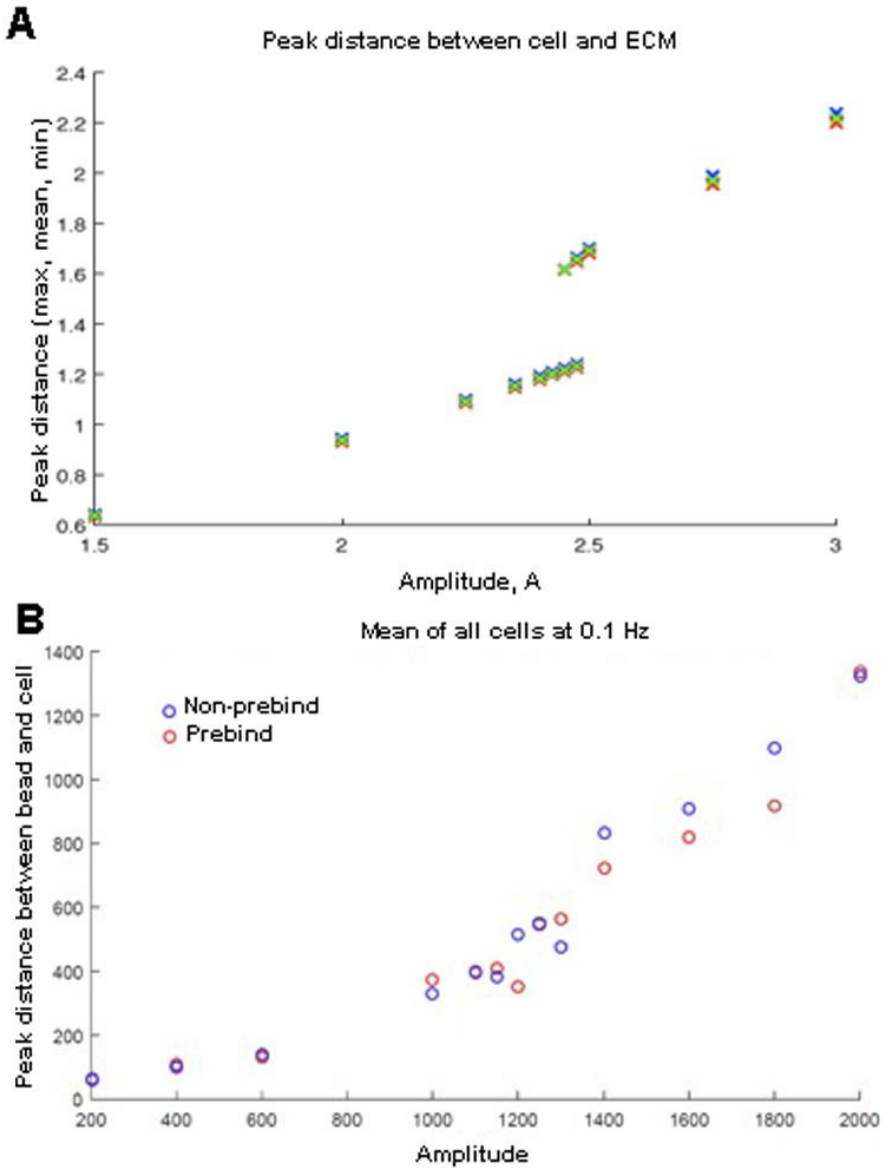

Figure 3-5. The cell-bead separation obtained from all amplitudes for the simulation model and biological data. (A) The cell-bead separation of simulation model. High separation (seen for high amplitude oscillations) indicates the full rupture state, whereas low separation (low amplitude oscillations) shows that adhesion dominates. There is a transition window of bistability (e.g., A-2.425, 2.475). This transition represents the point at which adhesion rupture abruptly dominates over adhesion as amplitude is increased. As the amplitude of the

oscillations approaches the low level, the separation approach to zero as in the low amplitude condition. (B) The cell-bead separation of experimental data. Compared with simulation model, data distribution showed similar pattern that transit point occurred around ramp size of 1400nm. Blue circle represents initial non-prebind condition and red circle represents prebind condition.

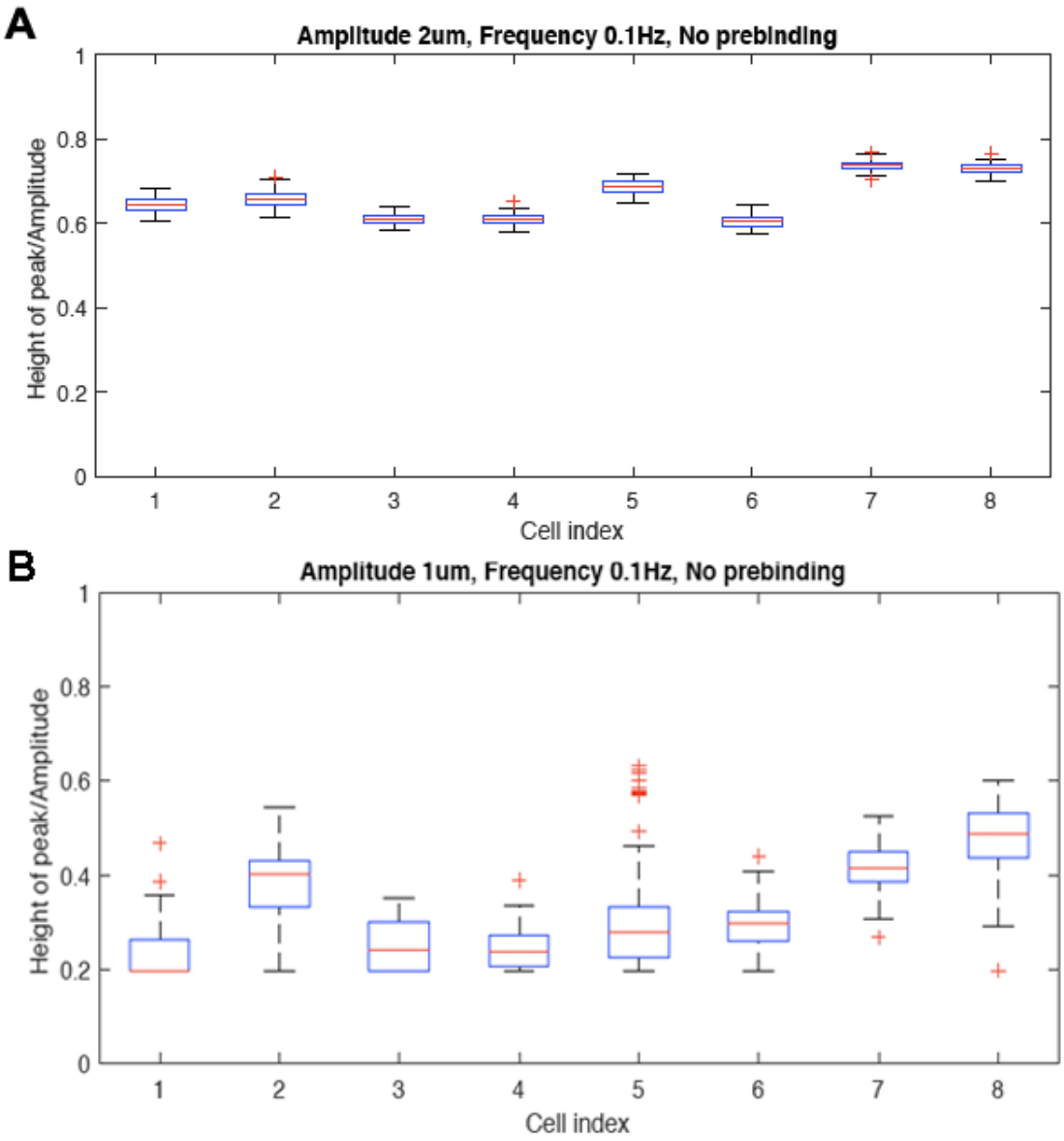

Figure 3-6. Boxplots of peak bead-cell separation for experimental oscillation of 1000 nm, and 2000 nm at 0.1 Hz in non-prebind initial condition. (A) Boxplots of peak bad-cell separation for 2000 nm. For this amplitude, all 8 cells have a high mean separation, and there is very little variation in this value, indicated by the low IQ range. (B) Boxplots of peak bead-cell separation for 1000 nm. For this amplitude, the mean bead-cell separation is much lower for all cells.

Figure 3-6 illustrates analysis of 1000 nm and 2000 nm amplitude oscillations under non-prebind conditions. The adhesion state was measured

by ratio of peak separation distance to amplitude. For experimental data with 2000 nm oscillations at 0.1Hz, all 8 cells produced similar behavior, with a consistently large bead-cell separation at each cycle due to a full rupture of all adhesions (Fig. 3-6A). In contrast, for experimental data using 1000 nm oscillations at 0.1Hz, the mean bead-cell separation is now much lower for all cells (Fig. 3-6B). Therefore, 1000 nm was selected as low amplitude for comparison to the simulation model and 2000 nm was used as the high amplitude for comparison with the model. The non-prebind and prebind data showed similar integrin adhesion behavior as predicted by the model at amplitudes of 1000 nm and 2000 nm. For other lower amplitudes, from 200 nm to 600 nm, separation of the FN-coated bead from the VSMC was not observed (data not shown). Peak bead-cell separation for experiments of all amplitudes from 200 nm to 2000 nm was plotted in Figure 3-7, and mean peak of prebind and non-prebind for each amplitude was compared statistically by two-sample Kolmogorv-Simirnov test. Mean peak bead-cell separation from amplitude of 1200 nm is significantly higher in non-pre-bind condition than the one in pre-bind condition at p level of 0.05.

Effect of cell compliance and model limitation

From the simulation model, a unique bistable behavior of integrin adhesion during intermediate amplitude displacement is predicted. One possibility is that this is due to multiple integrin adhesion cooperativity that in the model leads to differences in membrane deformation. With no existing integrin adhesion as the starting point there is less membrane deformation as the displacement cycle begins and the distance between cell and ECM separates quickly and therefore is larger leading to adhesion rupture. With pre-

existing integrin adhesions, there is a cooperativity and more membrane deformation with applied displacement and this distance is reduced. In the simulation model, stiffer cells were predicted to have longer separation distance of bead-cell at given amplitude, just as shown in Figure 3-8.

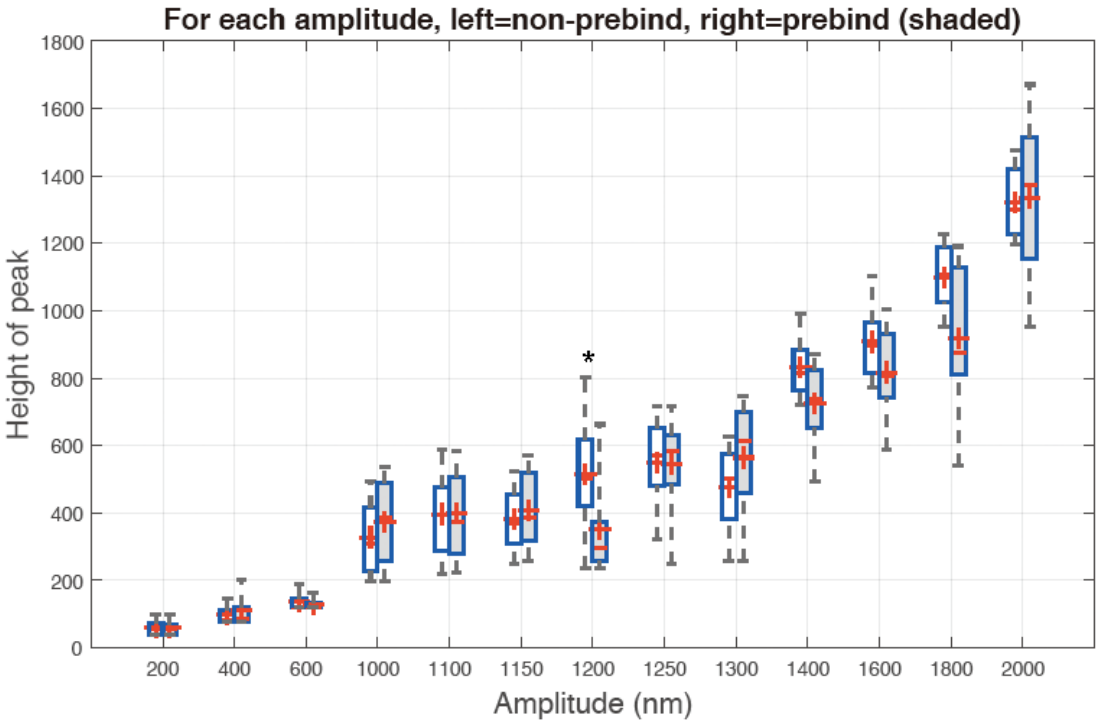

Figure 3-7. Boxplots of peak bead-cell separation for all experimental data in both non-prebind and prebind (shaded) initial conditions. Experimental data was collected from 200 nm to 2000 nm amplitude oscillations. At 1200 nm amplitude, mean peak bead-cell separation of non-prebind initial condition is significantly higher than that of prebind initial condition ($P < 0.05$).

The model designed for testing of an integrin focal adhesion interacting with the extracellular matrix (ECM) under deformation is a 3-spring model. The springs are represented by the vascular smooth muscle cell (VSMC), integirns and the ECM and each represented as linear springs with their own spring constants. Changes to any of these constants would lead to changes in the simulation outcomes and the nature of the bistable behavior. For example, VSMC stiffness would alter the level of cell deformation, which would affect the

distance between the cell and ECM. For compliant cells, more membrane deformation and a reduced distance between cell and ECM would be expected. Consequently, there is more integrin bond survival, and higher amplitudes of oscillation are needed to induce rupture, in other words the adhesions are more stable and can tolerate larger displacements and loads. These results suggest that changes in the cell compliance would alter the amplitude at which we see the high and low states, and therefore the position of a bistable region. However, further experimental work and model development is needed to see if stiffer VSMC exhibit changes in the bistable region.

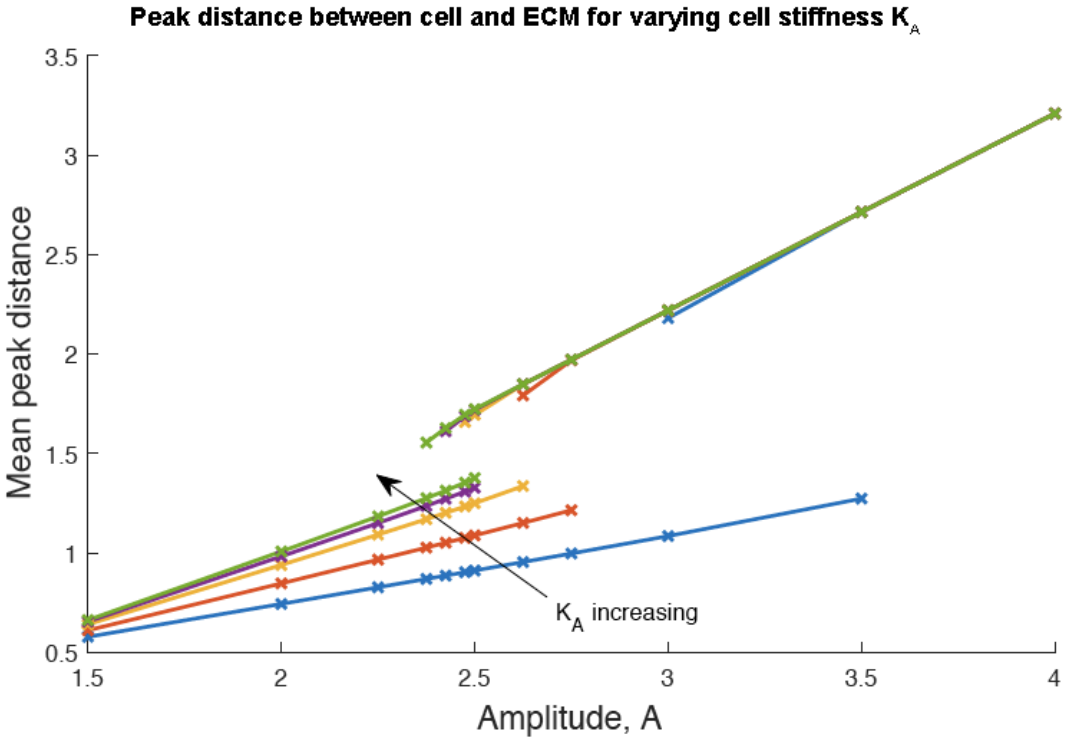

Figure 3-8. Effect of cell compliance on mean peak bead-cell separation distance for simulation model. K_A represents cell compliance that low K_A values indicates more compliant cells. For more compliance cells, a larger amplitude, A, is needed to induce rupture. Additionally, the separation distance is lower in compliant cells due to more cell deformation.

Many cardiovascular diseases are associated with changes in integrin expression, extracellular matrix (ECM) stiffness and vascular smooth muscle

cell (VSMC) stiffness [30, 84, 131]. Alteration of any of these values significantly changes the model predictions and from a pathophysiological point of view could significantly affect vascular function. As an example, collective evidence from our laboratory has demonstrated that cell stiffness can be correlated with integrin adhesion to ECM. VSMCs from normotensive animals that are less stiff than cells from hypertensive animals there is less adhesion to ECM whereas stiff cells exhibit enhanced cell adhesion to ECM [30].

Varying cell stiffness in the present model shows changes in integrin adhesion to vertical oscillations in the opposite way. Thus, these experimental data suggest there are multiple complexities (e.g. the inclusion of the cytoskeleton, which is absent in the model) to consider when trying to understand a cell's behavior to mechanical forces and the adaptations that take place. Again, this points to the need for more experimental data and additional modeling. Developing a fuller understanding will require continued collaboration of scientists from different disciplines.

CHAPTER IV

SUMMARY AND FUTURE DIRECTIONS

Integrins provide a physical bridge between the cytoskeleton and extracellular matrix proteins. This bridge of molecules is constantly exposed to mechanical and chemical stimuli from both inside and outside of the cells. Therefore, integrin adhesion to ECM must be a dynamically regulated response to the cellular microenvironment. In the vascular system, integrins have been demonstrated to play an important role in physiological and pathological conditions. Thus, investigation into the mechanisms governing adhesion of VSMC is important and necessary to achieve a better understanding of vascular disease. The work described in this series of studies focused on integrin adhesion in response to both chemical and mechanical stimulation.

The first series of studies describes work focused on trying to clarify cellular mechanisms that coordinate integrin adhesion with VSMC biomechanical status. This work concentrated on changes in integrin adhesion to FN with activation of VSMC to alter the contractile state and alter cell stiffness. My work suggests that intracellular Ca^{2+} involved in this coordination of adhesion with contraction/cellular mechanical state. However, mechanisms concerning how integrin adhesion was coordinated with cell stiffness are still not fully understood. Some areas of future study include investigating the specific calcium related signaling pathway or pathways that directly exert their effects on integrin adhesion or integrin associated proteins. Though cell stiffness is believed to be mostly governed by myosin-generated contractility, which is known to be regulated by intracellular level of Ca^{2+}, cytoskeleton remodeling also occurs in VSMCs following AII and cell contractile activation.

This suggest actin polymerization/depolymerizaton processes are an important area for future study and for further examining a role for Ca^{2+}. There are several good candidates that could be studied to determine role of actin remodeling in acute changes in stiffness following VSMC stimulation. One is calcium-calmodulin-dependent protein kinase II (CaMKII) that has been reported to regulate actin cytoskeletal assembly [116]. Additionally, actin polymerization is reported to be mediated through other pathways, such as RhoA. In relation to my studies, RhoA is also reported to be activated by AII [57]. Taken together with the fact that integrin engagement with the ECM also results in the activation of a vast spectrum of signaling pathways including small GTPase of the Rho family [63, 86] make this possibility attractive. Thus, it is clear that further studies would be needed to fully elucidate the precise signaling mechanism or mechanisms governing regulation of cellular mechanics and cell adhesion. To test possible involvement of RhoA/Rho kinase signaling pathway in AII-induced integrin activation, it is proposed that measurement of the active form of RhoA and total RhoA by western blotting after AII treatment. Possible RhoA targeted phosphorylated proteins would also be measured by western blotting. Another powerful approach would be to modulate expression of specific molecules, like RhoA, by overexpression or knockdown using shRNA. This would be a useful approach to identify whether changes in adhesion would be enhanced or suppressed.

In the second series studies conducted as part of this dissertation, my work focused on integrin adhesion responses to imposed mechanical oscillations. This study evolved out of a collaboration with Dr. Bindi Brook at the Department of Mathematical Sciences, University of Nottingham. As part of the

study, Dr. Brook and colleagues designed a mathematical model to describe the behavior of integrins in a focal adhesion during exposure to oscillatory mechanical force or stretch, such as might occur with pulse pressure. The model predicted unique integrin behavior emerging from the pattern of adhesion as the level of force or stretch on the adhesion was changed. This unique pattern was called ‘bistability”. In order to test these model predictions, my studies were designed to mimic the model simulations and collect actual biological data to either confirm or inform the model so it could be improved. Vertical oscillations were applied using AFM to test integrin adhesion behavior proposed in the mathematical simulation model. The results indicated that integrin behavior did display significant changes based on the initial state of integrin adhesion to the ECM and oscillation amplitudes (i.e. force/stretch). Since these simulations and experiments were conducted in the vertical direction and an important future direction is to explore integrin adhesion behavior when integrin adhesions are exposed to shearing or lateral force and stretch. VSMCs sense force not only vertically but also laterally so this is a physiologically relevant future direction for additional studies. How integrin adhesions in VSMC would respond to lateral oscillations has not yet been studied. Lateral oscillations can be performed by lateral force microscopy (LFM), which is also called friction force microscopy (FFM) and represents another operation mode in a standard AFM instrument working in contact mode [132]. In LFM, the cantilever is moved laterally over the investigated surface, and in this case, the interaction forces cause cantilever torsion, then the magnitude of the interaction forces can be determined by obtaining the force curves for torsion. Therefore, protocols performed in LFM are completely

different from normal AFM experiments, including calibration of cantilever, collecting and processing data. For LFM, the lateral force was determined by multiplying the recorded signal by the torsional spring constant and lateral photodetector sensitivity. Both parameters are difficult to estimate using traditional methods. To date, we have tried calibration of torsional spring constant with Sader methods [133, 134]. More work on collecting, analyzing and processing lateral data would be needed to complete lateral experiments.

Additionally, the proposed simulation model simply takes a whole cell as a spring that is constant throughout a simulation. However, cell membrane and cytoskeleton networks have different compliances and showed different behavior response to applied force that should not be considered as one spring. Thus, future refinement of the model should include more variables and parameters to represent these cellular constituents. Improvements such as this would likely improve the accuracy of the predictions and usefulness of the model. Moreover, in biological conditions, collective evidence has demonstrated cell stiffness changed the response to the dynamic microenvironment, including integrin activation and the bistable point. This may have significant implications in pathology where ECM and cell thickness have increased with consequential effects on signaling and vessel behavior.

It is of interest that the simulation model predicts a loss of focal adhesion stability as VSMC stiffness is enhanced. This has pathophysiological implications to hypertension and aging where VSMC stiffness is increased and suggest that these diseases may destabilize the focal adhesion and lead to a cycle of adaptive changes that lead to alteration in the ECM as well as adhesion molecule expression. In the simulation model Integrin expression is assumed

to remain constant. However, the literature reports that in chronic hypertension and aging that adhesion molecule expression is upregulated. It is reasonable to speculate the changes in expression may be a cellular mechanism to attempt to stabilize the focal adhesion so it will function normally. Thus, our simulation model informed on additional biological detail could be further refined to more accurately reflect the biological elements.

Besides adhesion of VSMC integrins to ECM proteins, cell-cell adhesion, mediated by cadherins, is also known important to maintain tissue structure and reported to regulate cellular signaling [135]. Therefore, future work would to study cell-cell adhesion responses to both vertical or lateral oscillations is also anticipated to yield important information relevant to VSMC behavior in the vascular wall. Moreover, there have been intracellular crosslinks identified between cadherin-mediated cell-cell adhesions and integrin-mediated cell-ECM adhesion that are important in signaling and integrating responses to mechanical forces [136]. In this case, building a new model to effect cadherin adhesion on integrin adhesion or vice versa would be necessary to help us understand the full picture of VSMCs adhesion behavior.

It is of interest that although the signaling role of integrins has been investigated extensively following integrin engagement or binding with ECM, there have been no studies to date that have focused on cellular signaling responses that might be entirely unique to rupture an integrin adhesion when it separates from an ECM binding site. The observed ‘bistable” behavior reported in this study suggest this would be a very novel and perhaps fruitful direction for future study. Since integrins are known to undergo dynamic regulation that includes spatial rearrangement on the cell surface recruitment to focal

adhesions [17], in this reverse process, integrin rupture could activate separate signal pathways in addition to turning off the classical out-side in pathways.

REFERENCES

1. http://www.who.int/mediacentre/factsheets/fs317/en/
2. Chaohong Li, Q.X., *Mechanical stree-initiated signal transductions in vascular smooth muscle cells.* Cellular Signalling, 2000. **12**: p. 11.
3. Jean, C., et al., *Influence of stress on extracellular matrix and integrin biology.* Oncogene, 2011. **30**(24): p. 2697-706.
4. Tracy, L.E., R.A. Minasian, and E.J. Caterson, *Extracellular Matrix and Dermal Fibroblast Function in the Healing Wound.* Adv Wound Care (New Rochelle), 2016. **5**(3): p. 119-136.
5. Clause, K.C. and T.H. Barker, *Extracellular matrix signaling in morphogenesis and repair.* Curr Opin Biotechnol, 2013. **24**(5): p. 830-3.
6. GM., C., *Cell walls and the Extracellular Matrix.* The Cell: A modelular Approach. 2000: Sunderland (MA): Sinauer Associates; .
7. Dinardo, C.L., et al., *Variation of mechanical properties and quantitative proteomics of VSMC along the arterial tree.* Am J Physiol Heart Circ Physiol, 2014. **306**(4): p. H505-16.
8. Ponticos, M. and B.D. Smith, *Extracellular matrix synthesis in vascular disease: hypertension, and atherosclerosis.* J Biomed Res, 2014. **28**(1): p. 25-39.
9. Wagenseil, J.E. and R.P. Mecham, *Vascular extracellular matrix and arterial mechanics.* Physiol Rev, 2009. **89**(3): p. 957-89.
10. Xu, J. and G.P. Shi, *Vascular wall extracellular matrix proteins and vascular diseases.* Biochim Biophys Acta, 2014.
11. Lu, P., et al., *Extracellular matrix degradation and remodeling in development and disease.* Cold Spring Harb Perspect Biol, 2011. **3**(12).

12. Moiseeva, E.P., *Adhesion receptors of vascular smooth muscle cells and their functions.* Cardiovasc Res, 2001. **52**: p. 15.

13. Martinez-Lemus, L.A., et al., *Integrins as Unique Receptors for Vascular Control.* Journal of Vascular Research, 2003. **40**(3): p. 211-233.

14. Martinez-Lemus, L.A., et al., *Integrins and regulation of the microcirculation: from arterioles to molecular studies using atomic force microscopy.* Microcirculation, 2005. **12**(1): p. 99-112.

15. Lacolley, P., et al., *Vascular Smooth Muscle Cells and Arterial Stiffening: Relevance in Development, Aging, and Disease.* Physiol Rev, 2017. **97**(4): p. 1555-1617.

16. Calderwood, D.A., *Integrin activation.* J Cell Sci, 2004. **117**(Pt 5): p. 657-66.

17. Welf, E.S., U.P. Naik, and B.A. Ogunnaike, *A spatial model for integrin clustering as a result of feedback between integrin activation and integrin binding.* Biophys J, 2012. **103**(6): p. 1379-89.

18. Nancy Hogg, R.H., Birgit Leitinger, Alison McDowall, Joanna Porter, Paula Stanley, *Mechanisms contributing to the activity of integrins on leukocytes.* Immunological Reviews, 2002. **186**: p. 8.

19. Broday, D.M., *Diffusion of clusters of transmembrane proteins as a model of focal adhesion remodeling.* Bull Math Biol, 2000. **62**(5): p. 891-924.

20. Malinin, N.L., E. Pluskota, and T.V. Byzova, *Integrin signaling in vascular function.* Curr Opin Hematol, 2012. **19**(3): p. 206-11.

21. Valencik, M.L., et al., *Integrin activation in the heart: a link between electrical and contractile dysfunction?* Circ Res, 2006. **99**(12): p. 1403-10.

22. Umesh, A., et al., *Alteration of pulmonary artery integrin levels in chronic hypoxia and monocrotaline-induced pulmonary hypertension.* J Vasc Res, 2011. **48**(6): p. 525-37.

23. Chao, J.T., *Modulation of 7-integrin-mediated adhesion and expression by platelet-derived growth factor in vascular smooth muscle cells.* AJP: Cell Physiology, 2005. **290**(4): p. C972-C980.

24. Egidius H.J. Heerkens, L.S., Alisdair Ryding, Gillian Brooker, John J. Mullins, Clare Austin, Vasken Ohanian, Anthony M. Heagerty, *aV Integrins are necessary for eutrophic inward remodelling of samll arteries in hypertension.* Hypertension, 2006. **47**(2): p. 7.

25. Laurent, S., et al., *Aortic stiffness as a tissue biomarker for predicting future cardiovascular events in asymptomatic hypertensive subjects.* Ann Med, 2012. **44 Suppl 1**: p. S93-7.

26. Kaess, B.M., et al., *Aortic stiffness, blood pressure progression, and incident hypertension.* JAMA, 2012. **308**(9): p. 875-81.

27. Bezie, Y., et al., *Fibronectin Expression and Aortic Wall Elastic Modulus in Spontaneously Hypertensive Rats.* Arteriosclerosis, Thrombosis, and Vascular Biology, 1998. **18**(7): p. 1027-1034.

28. Laurent, S., et al., *Expert consensus document on arterial stiffness: methodological issues and clinical applications.* Eur Heart J, 2006. **27**(21): p. 2588-605.

29. Reference Values for Arterial Stiffness, C., *Determinants of pulse wave velocity in healthy people and in the presence of cardiovascular risk factors: 'establishing normal and reference values'.* Eur Heart J, 2010. **31**(19): p. 2338-50.

30. Sehgel, N.L., et al., *Increased vascular smooth muscle cell stiffness: a novel mechanism for aortic stiffness in hypertension.* Am J Physiol Heart Circ Physiol, 2013. **305**(9): p. H1281-7.

31. Zhu, Y., et al., *Temporal analysis of vascular smooth muscle cell elasticity and adhesion reveals oscillation waveforms that differ with aging.* Aging Cell, 2012. **11**(5): p. 741-50.

32. GM, C., *Chapter 11, The Cytoskeleton and Cell Movement*, in *The Cell: A Molecular Approach*. 2000, Sinauer Associates: Sunderland (MA).

33. Zhang, S.J.G.a.W., *Actin cytoskeletal dynamics in smooth muscle: a new paradigm for the regulation of smooth muscle contraction.* Am J Physiol Cell Physiol, 2008. **295**(3): p. 12.

34. GM., C., *Actin, Myosin, and Cell Movement.*, in *The Cell: A Molecular Approach*. 2000, Sinauer Associates: Sunderland (MA).

35. Wu, Y. and S.J. Gunst, *Vasodilator-stimulated phosphoprotein (VASP) regulates actin polymerization and contraction in airway smooth muscle by a vinculin-dependent mechanism.* J Biol Chem, 2015. **290**(18): p. 11403-16.

36. Eisenmann, K.M., et al., *Dia-interacting protein modulates formin-mediated actin assembly at the cell cortex.* Curr Biol, 2007. **17**(7): p. 579-91.

37. Mutsuki Amano, M.N., Kozo Kaibuchi, *Rho-Kinase/ROCK: A Key Regulator of the Cytoskeleton and Cell Polarity.* Cytoskeleton (Hoboken), 2010. **67**(9): p. 10.

38. Hartmann, S., A.J. Ridley, and S. Lutz, *The Function of Rho-Associated Kinases ROCK1 and ROCK2 in the Pathogenesis of Cardiovascular Disease.* Front Pharmacol, 2015. **6**: p. 276.

39. Tang, D.D., *Intermediate filaments in smooth muscle.* Am J Physiol Cell Physiol, 2008. **294**(4): p. 10.

40. Tang, D.D. and B.D. Gerlach, *The roles and regulation of the actin cytoskeleton, intermediate filaments and microtubules in smooth muscle cell migration.* Respir Res, 2017. **18**(1): p. 54.

41. Ruping Wang, Q.L.a.D.D.T., *Role of vimentin in smooth muscle force development.* Am J Physiol Cell Physiol, 2006. **291**(3): p. 7.

42. Chitaley K, W.R., *Microtubule depolymerization facilitates contraction of rat aorta via activation of Rho-kinase.* Vascul Pharmacol., 2002. **38**(3): p. 5.

43. Lee, K., H. Kim, and D. Jeong, *Microtubule stabilization attenuates vascular calcification through the inhibition of osteogenic signaling and matrix vesicle release.* Biochem Biophys Res Commun, 2014. **451**(3): p. 436-41.

44. Brozovich, F.V., et al., *Mechanisms of Vascular Smooth Muscle Contraction and the Basis for Pharmacologic Treatment of Smooth Muscle Disorders.* Pharmacol Rev, 2016. **68**(2): p. 476-532.

45. Puetz, S., L.T. Lubomirov, and G. Pfitzer, *Regulation of smooth muscle contraction by small GTPases.* Physiology (Bethesda), 2009. **24**: p. 342-56.

46. Somlyo AP, S.A., *Ca2+ sensitivity of smooth muscle and nonmuscle myosin II: modulated by G proteins, kinases, and myosin phosphatase.* Physiol Rev, 2003. **83**(4): p. 34.

47. Mehta, P.K. and K.K. Griendling, *Angiotensin II cell signaling: physiological and pathological effects in the cardiovascular system.* Am J Physiol Cell Physiol, 2007. **292**(1): p. C82-97.

48. Widdop, R.E., et al., *Angiotensin AT2 receptors: cardiovascular hope or hype?* Br J Pharmacol, 2003. **140**(5): p. 809-24.

49. Dasgupta, C. and L. Zhang, *Angiotensin II receptors and drug discovery in cardiovascular disease.* Drug Discov Today, 2011. **16**(1-2): p. 22-34.

50. Montezano, A.C., et al., *Angiotensin II and vascular injury.* Curr Hypertens Rep, 2014. **16**(6): p. 431.

51. Wynne, B.M., C.W. Chiao, and R.C. Webb, *Vascular Smooth Muscle Cell Signaling Mechanisms for Contraction to Angiotensin II and Endothelin-1.* J Am Soc Hypertens, 2009. **3**(2): p. 84-95.

52. Do, K.H., et al., *Angiotensin II-induced aortic ring constriction is mediated by phosphatidylinositol 3-kinase/L-type calcium channel signaling pathway.* Exp Mol Med, 2009. **41**(8): p. 569-76.

53. Rama Natarajan, S.S., Wei Bai, Kiran Kumar V. Yerneni, Jerry Nadler, *Angiotensin II signaling in vascular smooth muscle cells under high glucose conditions.* Hypertension, 1999. **33**: p. 7.

54. Touyz RM, H.G., Deng LY, Schiffrin EL., *Role of extracellular signal-regulated kinases in angiotensin II-stimulated contraction of smooth muscle cells from human resistance arteries.* Circulation, 1999. **99**(3): p. 8.

55. XP, X., et al., *Central role of the MAPK pathway in ang II-mediated DNA synthesis and migration in rat vascular smooth muscle cells.* Arterioscler Thromb Vasc Biol, 1999. **19**(1): p. 10.

56. Wirth, A., *Rho kinase and hypertension.* Biochim Biophys Acta, 2010. **1802**(12): p. 1276-84.

57. Zeidan, A., et al., *Prevention of RhoA activation and cofilin-mediated actin polymerization mediates the antihypertrophic effect of adenosine recepotr agonist in angiotensin II- and endothelin- 1- treated cardiomyocytes.* Mol Cell Biochem, 2014. **385**(1-2): p. 239-48.

58. Loirand, G. and P. Pacaud, *The role of Rho protein signaling in hypertension.* Nat Rev Cardiol, 2010. **7**(11): p. 637-47.

59. Rajagopalan, S., et al., *Angiotensin II-mediated hypertension in the rat increases vascular superoxide production via membrane NADH/NADPH oxidase activation. Contribution to alterations of vasomotor tone.* J Clin Invest., 1996. **97**(8): p. 8.

60. KK, G., S. D, and U.-F. M., *NAD(P)H oxidase: role in cardiovascular biology and disease.* Circ Res, 2000. **86**(5): p. 8.

61. Nguyen Dinh Cat, A., et al., *Angiotensin II, NADPH oxidase, and redox signaling in the vasculature.* Antioxid Redox Signal, 2013. **19**(10): p. 1110-20.

62. Hong, Z., et al., *Vasoactive agonists exert dynamic and coordinated effects on vascular smooth muscle cell elasticity, cytoskeletal remodelling and adhesion.* J Physiol, 2014. **592**(Pt 6): p. 1249-66.

63. Peyton, S.R., et al., *The effects of matrix stiffness and RhoA on the phenotypic plasticity of smooth muscle cells in a 3-D biosynthetic hydrogel system.* Biomaterials, 2008. **29**(17): p. 2597-607.

64. Chaterji, S., et al., *Synergistic effects of matrix nanotopography and stiffness on vascular smooth muscle cell function.* Tissue Eng Part A, 2014. **20**(15-16): p. 2115-26.

65. Stegemann, J.P., H. Hong, and R.M. Nerem, *Mechanical, biochemical, and extracellular matrix effects on vascular smooth muscle cell phenotype.* J Appl Physiol (1985), 2005. **98**(6): p. 2321-7.

66. Hong, Z., et al., *Coordination of fibronectin adhesion with contraction and relaxation in microvascular smooth muscle.* Cardiovasc Res, 2012. **96**(1): p. 73-80.

67. Davis MJ, W.X., Nurkiewicz TR, Kawasaki J, Davis GE, Hill MA, Meininger GA, *Integrin and mechanotransduction of the vascular myogenic reponse.* Am J Phsiol Heart Circ Physiol, 2001. **280**(4): p. 7.

68. Wu, X., et al., *Regulation of the L-type calcium channel by alpha 5beta 1 integrin requires signaling between focal adhesion proteins.* J Biol Chem, 2001. **276**(32): p. 30285-92.

69. Xin Wu, J.E.M., Steven H. Platts, George E. Davis, Gerald A. Meininger, and Michael J. Davis, *Modulation of calcium current in arteriolar smooth muscle by avb3 and a5b1 integrin ligands.* The Journal of Cell Biology, 1998. **14**: p. 12.

70. Waitkus-Edwards, K.R., *alpha4beta1 Integrin Activation of L-Type Calcium Channels in Vascular Smooth Muscle Causes Arteriole Vasoconstriction.* Circulation Research, 2002. **90**(4): p. 473-480.

71. Hahn, C. and M.A. Schwartz, *Mechanotransduction in vascular physiology and atherogenesis.* Nat Rev Mol Cell Biol, 2009. **10**(1): p. 53-62.

72. Francis, L.W., et al., *Atomic force microscopy comes of age.* Biol Cell, 2009. **102**(2): p. 133-43.

73. Carvalho, F.A. and N.C. Santos, *Atomic force microscopy-based force spectroscopy--biological and biomedical applications.* IUBMB Life, 2012. **64**(6): p. 465-72.

74. Kalle, W. and P. Strappe, *Atomic force microscopy on chromosomes, chromatin and DNA: a review.* Micron, 2012. **43**(12): p. 1224-31.

75. Carvalho, F.A., I.C. Martins, and N.C. Santos, *Atomic force microscopy and force spectroscopy on the assessment of protein folding and functionality.* Arch Biochem Biophys, 2013. **531**(1-2): p. 116-27.

76. Wang, C. and V.K. Yadavalli, *Investigating biomolecular recognition at the cell surface using atomic force microscopy.* Micron, 2014. **60**: p. 5-17.

77. Benitez, R. and J.L. Toca-Herrera, *Looking at cell mechanics with atomic force microscopy: experiment and theory.* Microsc Res Tech, 2014. **77**(11): p. 947-58.

78. Zhang, J., et al., *Single molecular recognition force spectroscopy study of a luteinizing hormone-releasing hormone analogue as a carcinoma target drug.* J Phys Chem B, 2012. **116**(45): p. 13331-7.

79. van Es, M.H., et al., *Single molecule binding dynamics measured with atomic force microscopy.* Ultramicroscopy, 2014. **140**: p. 32-6.

80. Karacsony, O. and B.B. Akhremitchev, *On the detection of single bond ruptures in dynamic force spectroscopy by AFM.* Langmuir, 2011. **27**(18): p. 11287-91.

81. Puchner, E.M. and H.E. Gaub, *Force and function: probing proteins with AFM-based force spectroscopy.* Curr Opin Struct Biol, 2009. **19**(5): p. 605-14.

82. Whited, A.M. and P.S. Park, *Atomic force microscopy: a multifaceted tool to study membrane proteins and their interactions with ligands.* Biochim Biophys Acta, 2014. **1838**(1 Pt A): p. 56-68.

83. Andolfi, L., et al., *Investigation of adhesion and mechanical properties of human glioma cells by single cell force spectroscopy and atomic force microscopy.* PLoS One, 2014. **9**(11): p. e112582.

84. Evans, P.C., et al., *Biomechanics in vascular biology and cardiovascular disease.* Thromb Haemost, 2016. **115**(3): p. 465-6.

85. Saphirstein, R.J., et al., *The focal adhesion: a regulated component of aortic stiffness.* PLoS One, 2013. **8**(4): p. e62461.

86. Lim, S.M., et al., *RhoA-induced cytoskeletal tension controls adaptive cellular remodeling to mechanical signaling.* Integr Biol (Camb), 2012. **4**(6): p. 615-27.

87. J. Geoffrey Pickering, L.H.C., Shaohua Li, Kem A. Rogers, Edward F. Rocnik, Rober Zhong, and Bosco M. C. Chan, *a5b1 Integrin expression and luminal edge fibronectin matrix assembly by smooth muscle cells after arterial injury.* American Journal of Pathology, 2000. **156**(2): p. 13.

88. Sun, Z., et al., *Mechanical properties of the interaction between fibronectin and alpha5beta1-integrin on vascular smooth muscle cells studied using atomic force microscopy.* Am J Physiol Heart Circ Physiol, 2005. **289**(6): p. H2526-35.

89. Francis, S.E., *Central Roles of alpha5beta1 Integrin and Fibronectin in Vascular Development in Mouse Embryos and Embryoid Bodies.* Arteriosclerosis, Thrombosis, and Vascular Biology, 2002. **22**(6): p. 927-933.

90. Lee, D.Y., et al., *Oscillatory flow-induced proliferation of osteoblast-like cells is mediated by alphavbeta3 and beta1 integrins through synergistic interactions of focal adhesion kinase and Shc with phosphatidylinositol 3-kinase and the Akt/mTOR/p70S6K pathway.* J Biol Chem, 2010. **285**(1): p. 30-42.

91. Sarrazy, V., et al., *Integrins alphavbeta5 and alphavbeta3 promote latent TGF-beta1 activation by human cardiac fibroblast contraction.* Cardiovasc Res, 2014. **102**(3): p. 407-17.

92. Paszek, M.J., et al., *The cancer glycocalyx mechanically primes integrin-mediated growth and survival.* Nature, 2014. **511**(7509): p. 319-25.

93. Platts SH, M.J., Davis MJ, Meininger GA., *Role fo k+ channels in arteriolar vasodilation mediated by integrin interaction with RGD-containing peptide.* Am J Physiol., 1998.

94. G. D'Angelo , J.E.M., G. E. Davis , M. J. Davis , G. A. Meininger, *Integrin-mediated reduction in vascular smooth muscel calcium induced by RGD-containing peptide.* AJP - Heart and Circulatory Physiology, 1997. **272**.

95. Mogford, J.E., et al., *Vascular Smooth Muscle v 3 Integrin Mediates Arteriolar Vasodilation in Response to RGD Peptides.* Circulation Research, 1996. **79**(4): p. 821-826.

96. Trache, A., et al., *Histamine effects on endothelial cell fibronectin interaction studied by atomic force microscopy.* Biophys J, 2005. **89**(4): p. 2888-98.

97. Hong, Z., et al., *Vascular smooth muscle cell stiffness and adhesion to collagen I modified by vasoactive agonists.* PLoS One, 2015. **10**(3): p. e0119533.

98. Banno, A. and M.H. Ginsberg, *Integrin activation.* Biochem Soc Trans, 2008. **36**(Pt 2): p. 229-34.

99. Askari, J.A., et al., *Focal adhesions are sites of integrin extension.* J Cell Biol, 2010. **188**(6): p. 891-903.

100. Julie C. Friedland, M.H.L., David Boettiger, *Mechanically activated integrin switch controls a5b1 function.* Sience, 2009. **323**(5914): p. 3.

101. Kong, F., et al., *Demonstration of catch bonds between an integrin and its ligand.* J Cell Biol, 2009. **185**(7): p. 1275-84.

102. Smith, B.A., et al., *Probing the viscoelastic behavior of cultured airway smooth muscle cells with atomic force microscopy: stiffening induced by contractile agonist.* Biophys J, 2005. **88**(4): p. 2994-3007.

103. Baumgartner, W., et al., *Cadherin interaction probed by atomic force microscopy.* Proc Natl Acad Sci U S A, 2000. **97**(8): p. 4005-10.

104. Jackson WF, H.J., Rusch NJ., *Enzymatic isolation and characterization of single vascular smooth muscle cells from creamsteric arterioles.* Microcirculation, 1997. **4**(1): p. 15.

105. S.S.M. Rensen, P.A.F.M.D., G.J.J. van Eys, *Regulation and characteristics of vascular smooth muscle cell phenotypic diversity.* Netherlands Heart Journal, 2007. **15**(3): p. 9.

106. Simo-Cheyou, E.R., et al., *STIM-1 and ORAI-1 channel mediate angiotensin-II-induced expression of Egr-1 in vascular smooth muscle cells.* J Cell Physiol, 2017. **232**(12): p. 3496-3509.

107. Schiffrin, R.M.T.a.E.L., *Signal Transduction Mechanisms Mediating the Physiological and Pathophysiological Actions of Angiotensin II in Vascular Smooth Muscle Cells.* Pharmacol Rev, 2000. **52**(4): p. 4.

108. Misárková E, B.M., Bencze M, Zicha J., *Excitation-contraction coupling and excitation-transcription coupling in blood vessels: their possible interactions in hypertensive vascular remodeling.* Physiol. Res., 2016. **65**: p. 9.

109. Yamin, R. and K.G. Morgan, *Deciphering actin cytoskeletal function in the contractile vascular smooth muscle cell.* J Physiol, 2012. **590**(Pt 17): p. 4145-54.

110. Fabry, B., et al., *Focal adhesion kinase stabilizes the cytoskeleton.* Biophys J, 2011. **101**(9): p. 2131-8.

111. Gardel, M.P.M.a.M.L., *F-actin buckling coordinates contractility and serving in a biomimetic actomyosin cortex.* PNAS, 2012. **109**(51): p. 16.

112. Field, C.M. and P. Lenart, *Bulk cytoplasmic actin and its functions in meiosis and mitosis.* Curr Biol, 2011. **21**(19): p. R825-30.

113. Munjal, A. and T. Lecuit, *Actomyosin networks and tissue morphogenesis.* Development, 2014. **141**(9): p. 1789-93.

114. Reymann, A.C., et al., *Actin network architecture can determine myosin motor activity.* Science, 2012. **336**(6086): p. 1310-4.

115. Saphirstein, R.J., et al., *Cortical actin regulation modulates vascular contractility and compliance in veins.* J Physiol, 2015. **593**(17): p. 3929-41.

116. Hoffman, L., M.M. Farley, and M.N. Waxham, *Calcium-calmodulin-dependent protein kinase II isoforms differentially impact the dynamics and structure of the actin cytoskeleton.* Biochemistry, 2013. **52**(7): p. 1198-207.

117. Huber, A. and S.F. Badylak, *Phenotypic changes in cultured smooth muscle cells: limitation or opportunity for tissue engineering of hollow organs?* J Tissue Eng Regen Med, 2012. **6**(7): p. 505-11.

118. Chang, S., et al., *Phenotypic modulation of primary vascular smooth muscle cells by short-term culture on micropatterned substrate.* PLoS One, 2014. **9**(2): p. e88089.

119. Caswell, P.T., S. Vadrevu, and J.C. Norman, *Integrins: masters and slaves of endocytic transport.* Nat Rev Mol Cell Biol, 2009. **10**(12): p. 843-53.

120. Lehoux S, T.A., *Signal transduction of mechanical stresses in the vascular wall.* Hypertension, 1998. **32**(2): p. 8.

121. Bryan, M.T., et al., *Mechanoresponsive networks controlling vascular inflammation.* Arterioscler Thromb Vasc Biol, 2014. **34**(10): p. 2199-205.

122. Kutys, M.L. and C.S. Chen, *Forces and mechanotransduction in 3D vascular biology.* Curr Opin Cell Biol, 2016. **42**: p. 73-79.

123. Anwar, M.A., et al., *The effect of pressure-induced mechanical stretch on vascular wall differential gene expression.* J Vasc Res, 2012. **49**(6): p. 463-78.

124. Martin A. Schwartz, M.D.S., Mark H. Ginsberg, *Integrins: emerging paradigms of signal transduction.* Annu Rev Cell Dev Biol, 1995. **11**(1): p. 51.

125. Vogel, V. and M. Sheetz, *Local force and geometry sensing regulate cell functions.* Nat Rev Mol Cell Biol, 2006. **7**(4): p. 265-75.

126. Chaohong Li, Q.X., *Mechanical stress-initiated signal transductions in vascular smooth muscle cells.* Cellular Signalling, 2000. **12**: p. 11.

127. Sun, Z., et al., *Extracellular matrix-specific focal adhesions in vascular smooth muscle produce mechanically active adhesion sites.* Am J Physiol Cell Physiol, 2008. **295**(1): p. C268-78.

128. Vernerey, F.J. and M. Farsad, *A mathematical model of the coupled mechanisms of cell adhesion, contraction and spreading.* J Math Biol, 2014. **68**(4): p. 989-1022.

129. Kathleen P. Wilkie, G.N., and Miles Johnston, *A mathematical analysis of physiological and molecular mechanisms that modulate pressure gradients and facilitate ventricular expansion in hydrocephalus.* Int J Numer Anal Model B., 2012. **316**: p. 17.

130. Gary K. Owens, A.L., David Gordon, and Maria M, Thompson, *Expression of smooth muscle-specific alpha-isoactin in cultured vascular smooth muscle cells: relationship between growth and cytodifferentiation.* The Journal of Cell Biology, 1986. **102**(2): p. 10.

131. Freedman, B.R., et al., *The (dys)functional extracellular matrix.* Biochim Biophys Acta, 2015. **1853**(11 Pt B): p. 3153-64.

132. Kulik, A.J., et al., *Probing fibronectin-antibody interactions using AFM force spectroscopy and lateral force microscopy.* Beilstein J Nanotechnol, 2015. **6**: p. 1164-75.

133. Rachel J. Cannara, M.E., Robert W. Carpick, *Lateral force calibration in atomic force microscopy: A new lateral force calibration method and general guidelines for optimization.* Departmental Papers (MEAM), 2006. **84**.

134. Tran Khac, B.C. and K.H. Chung, *Quantitative assessment of contact and non-contact lateral force calibration methods for atomic force microscopy.* Ultramicroscopy, 2016. **161**: p. 41-50.

135. Sun, Z., et al., *N-cadherin, a vascular smooth muscle cell-cell adhesion molecule: function and signaling for vasomotor control.* Microcirculation, 2014. **21**(3): p. 208-18.

136. Mui, K.L., C.S. Chen, and R.K. Assoian, *The mechanical regulation of integrin-cadherin crosstalk organizes cells, signaling and forces.* J Cell Sci, 2016. **129**(6): p. 1093-100.

VITA

Huang Huang was born on May 28th, 1986 in Jiangsu, China. She is daughter of Zefei Huang and Shuqin Zheng. Huang finished her Bachelor and Master degrees in Biological Science from Nanjing University, China, in 2011. In the fall of 2011, she joined the Department of Medical Pharmacology and Physiology at the University of Missouri-Columbia. She received her Ph.D in December 2017.